

# Beyond maps: Patterns of formation processes at the Middle Pleistocene open-air site of Marathousa 1, Megalopolis Basin, Greece

D. Giusti<sup>a,\*</sup>, V. Tourloukis<sup>a</sup>, G. E. Konidaris<sup>a</sup>, N. Thompson<sup>a</sup>, P. Karkanas<sup>b</sup>, E. Panagopoulou<sup>c</sup>, K. Harvati<sup>a</sup>

<sup>a</sup>*Paläoanthropologie, Senckenberg Centre for Human Evolution and Palaeoenvironment, Eberhard Karls Universität Tübingen, Rümelinstr. 23, 72070 Tübingen, Germany*

<sup>b</sup>*Malcolm H. Wiener Laboratory for Archaeological Science, American School of Classical Studies at Athens, Greece*

<sup>c</sup>*Ephoreia of Palaeoanthropology-Speleology of Greece, Athens, Greece*

---

## Abstract

Recent excavations at the Middle Pleistocene open-air site of Marathousa 1 have unearthed in one of the two investigated areas (Area A) a partial skeleton of a single individual of *Elephas (Palaeoloxodon) antiquus* and other faunal remains in spatial and stratigraphic association with lithic artefacts. In Area B, a much higher number of lithic artefacts was collected, spatially and stratigraphically associated with other faunal remains. The two areas are stratigraphically correlated, the main fossiliferous layers representing an *en masse* depositional process in a lake margin context. Evidence of butchering (cut-marks) has been identified on two bones of the elephant skeleton, as well on other mammal bones from Area B. However, due to the secondary deposition of the main find-bearing units, it is of primary importance to evaluate the degree and reliability of the spatial association of the lithic artefacts with the faunal remains. Indeed, spatial association does not necessarily imply causation, since natural syn- and post-depositional processes may equally produce spatial association. Assessing the degree and extent of post-depositional reworking processes is crucial to fully comprehend the archaeological record, and therefore to reliably interpret past human behaviours. The present study uses a comprehensive set of spatial statistics in order to disentangle the depositional processes behind the distribution of the archaeological and palaeontological record at Marathousa 1. Preliminary results of our analyses suggest minor reworking and substantial spatial association of the lithic and faunal assemblages, supporting the current interpretation of Marathousa 1 as a butchering site.

**Keywords:** Spatial analysis, Site formation processes, Vertical distribution, Fabric analysis, Point pattern analysis, Middle Pleistocene

---

\*Corresponding author

Email address: domenico.giusti@uni-tuebingen.de (D. Giusti)

1      **1. Introduction**

2      Archaeological site formation processes, intensively studied since the early 1970s  
3    ([Isaac, 1967](#); [Schiffer, 1972, 1983, 1987](#); [Shackley, 1978](#); [Wood and Johnson, 1978](#);  
4    [Binford, 1981](#); [Schick, 1984, 1986, 1987](#); [Petraglia and Nash, 1987](#); [Petraglia and](#)  
5    [Potts, 1994](#), among others), “still insufficiently taken in consideration” ([Texier, 2000](#),  
6    p.379) at the beginning of the 21st century, are nowadays fully acknowledged in the ar-  
7    chaeological practice ([Villa, 2004](#); [Bailey, 2007](#); [Brantingham et al., 2007](#); [Malinsky-](#)  
8    [Buller et al., 2011](#); [Vaquero et al., 2012](#); [Bargalló et al., 2016](#), among others). Drawing  
9    inferences about past human behaviours from scatters of archaeological remains must  
10   account for syn- and post-depositional contextual processes.

11     Several methods are currently applied in order to qualify and quantify the type and  
12   degree of reworking of archaeological assemblages. Within the framework of a geoar-  
13   chaeological and taphonomic approach, spatial statistics offer meaningful contributions  
14   in unravelling site formation and modification processes from spatial patterns. How-  
15   ever, while the spatio-temporal dimension is an ineluctable inherent property of any  
16   biotic and abiotic process, spatial statistics are still insufficiently applied.

17     Distribution maps are cornerstones of the archaeological documentation process  
18   and are primary analytic tools. However, their visual interpretation is prone to subjec-  
19   tivity and is not reproducible ([Bevan et al., 2013](#)). Since the early 1970's (see [Hodder](#)  
20   and [Orton \(1976\)](#); [Orton \(1982\)](#) and references therein), the traditional, intuitive, ‘eye-  
21   balling’ method of spotting spatial patterns has been abandoned in favour of more ob-  
22   jective approaches, extensively borrowed from other fields. Nevertheless, quantitative  
23   methods, while still percolating in the archaeological sciences from neighbouring dis-  
24   ciplines, are not extensively used. Moreover, only a relatively small number of studies  
25   have explicitly applied spatial point pattern analysis or geostatistics to the study of site  
26   formation and modification processes ([Lenoble et al. \(2008\)](#); [Domínguez-Rodrigo et al.](#)  
27   ([2014b,a, 2017](#)); [Carrer \(2015\)](#); [Giusti and Arzarello \(2016\)](#); [Organista et al. \(2017\)](#) -  
28   but see [Hivernel and Hodder \(1984\)](#) for an earlier work on the subject).

29     The goal of a taphonomic approach to spatial analysis is to move beyond distri-  
30   bution maps by applying a comprehensive set of multiscale and multivariate spatial  
31   statistics in order to reliably construct inferences from spatial patterns. An exhaustive  
32   spatial analytic approach to archaeological inference, combined with a taphonomic  
33   perspective, is essential for evaluating the depositional processes and integrity of the  
34   archaeological assemblage, and consequently for a reliable interpretation of past hu-  
35   man behaviours.

36     The present study uses a comprehensive set of spatial statistics in order to disentan-  
37   gle the depositional processes behind the spatial distribution of the archaeological and  
38   palaeontological record recovered during excavation at the Middle Pleistocene open-air  
39   site of Marathousa 1, Megalopolis, Greece ([Panagopoulou et al., 2015](#); [Harvati et al.](#),  
40   [2016](#)).

41      **1.1. Marathousa 1**

42     The site (Fig. 1), discovered in 2013 at the edge of an active lignite quarry (?), is  
43   located between two lignite seams in the Pleistocene deposits of the Megalopolis basin,  
44   Marathousa Member of the Choremi Formation ([van Vugt et al., 2000](#)). The regular

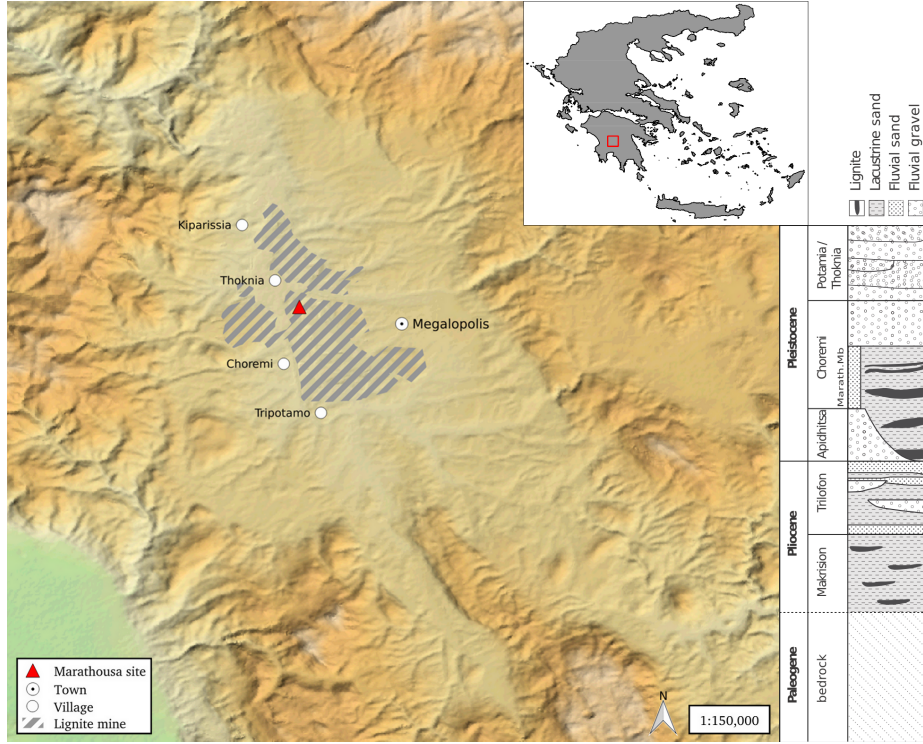


Figure 1: Geographical location of the Marathousa 1 site in the Megalopolis basin and stratigraphic column of the basin, modified after [van Vugt et al. \(2000\)](#).

45 alternation of lacustrine clay, silt and sand beds with lignite seams has been interpreted  
 46 having cyclic glacial (or stadial) and interglacial (or interstadial) origin ([Nickel et al., 1996](#)). The half-graben configuration of the basin, with major subsidence along the  
 47 NW-SE trending normal faults along the eastern margin, resulted in the gentle dip of  
 48 the lake bottom at the opposite, western, margin of the lake, enabling the formation of  
 49 swamps and the accumulation of organic material for prolonged periods of time ([van  
 50 Vugt et al., 2000](#)).

51 Two excavation areas have been investigated since 2013 (Fig. 2): Area A, where  
 52 several skeletal elements of a single individual of *Elephas (Palaeoloxodon) antiquus*  
 53 have been unearthed, together with a number of lithic artefacts; and Area B, located  
 54 60 m to the South along the exposed section, where the lithic assemblage is richer and  
 55 occurs in association with a faunal assemblage composed of isolated elephant bones,  
 56 cervids and carnivores among others ([Konidaris et al., this issue](#); [Tourloukis et al., this issue](#)). Evidence of butchering (cut-marks) have been identified on two of the  
 57 elephant bones from Area A, as well on elephant and other mammal bones from Area  
 58 B ([Konidaris et al., this issue](#)).

59 The sedimentary sequence of the site (Fig. 3) includes lacustrine and fluvio-lacustrine  
 60 clastic deposits between lignite seam II (UA7-UB10) and the lower part of seam III

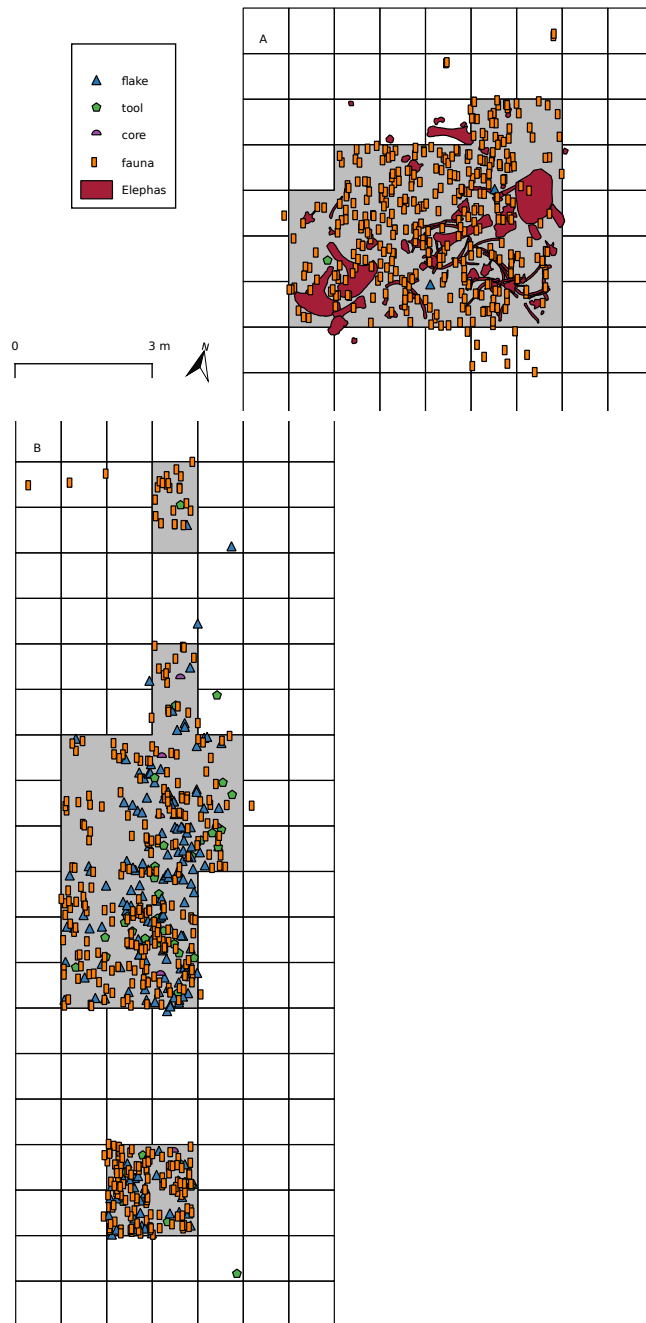


Figure 2: Distribution maps of the remains in Area A and Area B. Grey zone marks the 2015 excavation areas. Area B is located 60 m to the South, along the exposed section of the lignite quarry.

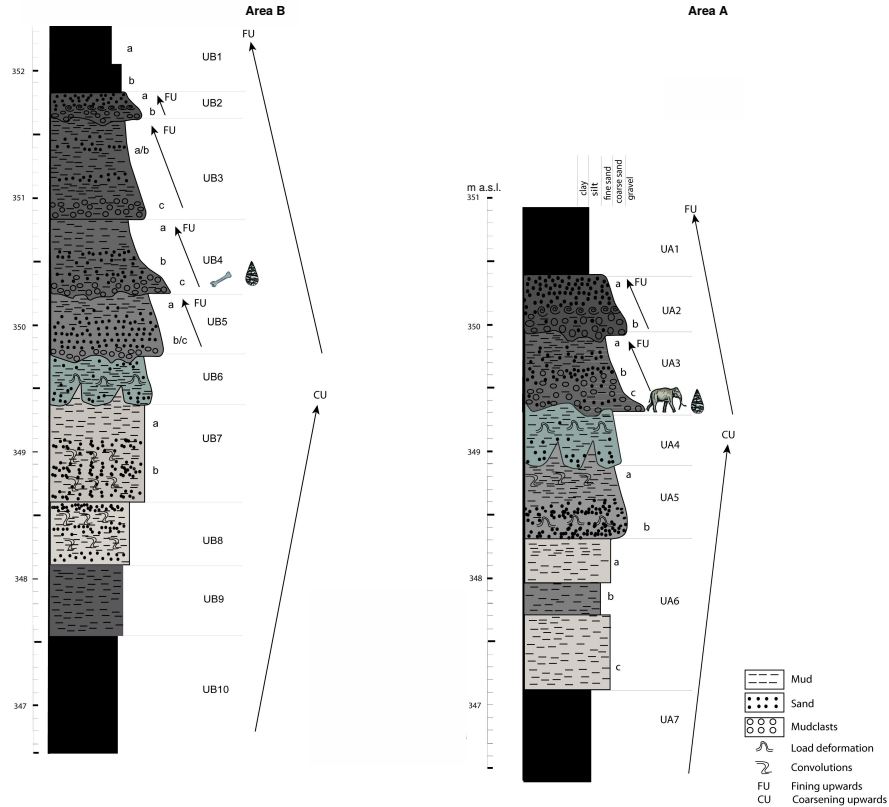


Figure 3: Stratigraphic setting of the Marathousa 1 site, modified after Karkanas et al. (this issue).

(UA1-UB1) (Karkanas et al., this issue; Tourloukis et al., this issue). A major hiatus (UA3/4, UB5/6), attributed to exposure and erosion of a lake shore mudflat, divides the sequence in two parts. The lower part is characterized by relatively high rate subaqueous sedimentation of bedded sands and silts, containing low organic and carbonate content. The upper one is characterized by a series of erosional bounded depositional units, attributed to subaerial organic- and carbonate-rich mudflows and hyperconcentrated flows (Karkanas et al., this issue).

The erosional contacts UA3c/4 and UB4c/5a separate the two main find-bearing units in both areas. In Area A, the elephant remains lie at the contact of UA3c/4 and are covered by UA3c (Fig. 4a); while in Area B, most of the remains were collected from unit UB4c (Fig. 4b). Units UA3c and UB4c (organic- and intraclast-rich silty sands) resemble dilute mudflows, showing a chaotic structure of rip-up clasts from the underlying unit, small-to-large wood fragments and rare rock clasts. In Area B, a relatively low number of remains was also found in massive organic-rich silty sands (UB5a), which locally overlay channalized sands (UB5b/c), probably not preserved in



Figure 4: Photograph (2017) of the left femur of the *Elephas (Palaeoloxodon) antiquus*, lying at the UA3c/4 contact and covered by unit UA3c (a). West profile (2014) of the excavation Area B (square 932/603), exposing the UB4c/5a and UB5c/6 erosional contacts (b).

78     Area A (Karkanas et al., this issue).

79     The flow event described above (units UA3c and UB4c), and specifically the ero-  
80     sional contacts between the fossiliferous horizons in the two areas (UA3c/4 and UB4c/5a),  
81     provide the essential background for the analysis and interpretation of the spatial dis-  
82     tributions at Marathousa 1.

83     The secondary depositional nature of the main find horizons raises the question of  
84     how reliable is the spatial association between the lithic artefacts and the partial skele-  
85     ton of a single *Elephas (Palaeoloxodon) antiquus* individual and other faunal remains.  
86     Since spatial association does not necessarily imply causation, and consequently syn-  
87     chrony, the answer has important consequences for the interpretation of the site in the  
88     broader context of the Middle Pleistocene human-proboscidean interactions. We aim  
89     to tackle this question and disentangle the formation processes acting at Marathousa 1  
90     on the basis of spatial patterns through a three-prong spatial analytic approach:

- 91       1. by analysing, in a frame of references, the orientation patterns of remains from  
92       relevant stratigraphic units;  
93       2. by quantifying and comparing their relative vertical distributions;  
94       3. by identifying spatial trends in either the assemblage intensities and the associa-  
95       tions between classes of remains.

96       Two contrasting hypotheses are tested: the autochthonous hypothesis (*sensu* Fernández-  
97       López, 1991; Domínguez-Rodrigo et al., 2012) states that the flow event, represented  
98       by units UA3c and UB4c, eroded and scoured the exposed surface (where the elephant

99 was lying), thereby entraining clastic material (including artefacts) and re-depositing  
100 (*sensu* Fernández-López, 1991) this material at a close distance. This model implies the  
101 loss of any original, pristine spatial relations between remains, but minor transport from  
102 the primary depositional *loci*. On the other hand, the allochthonous hypothesis (*sensu*  
103 Fernández-López, 1991; Domínguez-Rodrigo et al., 2012) implies significant transport  
104 from the original *loci* of deposition and re-elaboration (*sensu* Fernández-López, 1991).  
105 According to this model, the spurious spatial association between the lithic artefacts  
106 and faunal remains does not support any behavioural interpretation.

107 **2. Material and methods**

108 Since 2013, systematic investigation of the Marathousa 1 site has been carried out  
109 by a joint team from the Ephoreia of Palaeoanthropology-Speleology (Greek Ministry  
110 of Culture) and the University of Tübingen. A grid system of 1 square meter units  
111 was set up, oriented -14 degrees off the magnetic North, and including the two areas  
112 of investigation. The excavation of the deposit proceeded in 50x50 cm sub-squares  
113 in Area B and 1x1 m squares in Area A, and spits of 5 to 10 cm thickness, respec-  
114 tively. Systematic water-screening of sediments was carried out on-site using 1 mm  
115 sieves in order to guarantee recovery of the small-size fraction (e.g., micro-artefacts,  
116 small mammal remains, fish, molluscs and small fragments of organic and inorganic  
117 material). The three-dimensional coordinates of finds (i.e., all the lithic artefacts, teeth  
118 and diagnostic bones; bones and organic material with a-axis  $\geq$  20 mm), collected  
119 spits of sediment, samples and geological features (e.g., erosional contacts and mud  
120 cracks) were recorded with a Total Station. Dense clouds of surface points of the ele-  
121 phant skeletal elements were acquired using both a Total Station and a close-range  
122 photogrammetric technique.

123 The dimensions (length, width and thickness) of registered finds were measured  
124 on-site with millimetre rules. Orientation (plunge and bearing) of elongated particles  
125 (i.e., faunal remains, large wood fragments and lithic artefacts) was recorded since  
126 2013 using a clock-like system (the bearing was measured, relatively to the grid North,  
127 in twelve clockwise intervals of 30°; the plunge with a 22.5° accuracy). In 2015, the  
128 use of a compass and inclinometer with an accuracy of 1° was introduced in Area B to  
129 gradually replace the former method.

130 The widespread use of a compass and inclinometer to record orientation data (Voorhies,  
131 1969; Fiorillo, 1991; Bertran and Texier, 1995; Bertran et al., 1997; Lenoble and  
132 Bertran, 2004; Eberth et al., 2007; Eren et al., 2010; Benito-Calvo et al., 2011; Domínguez-  
133 Rodrigo et al., 2012; Domínguez-Rodrigo and García-Pérez, 2013; Domínguez-Rodrigo  
134 et al., 2014c; Cobo-Sánchez et al., 2014; Organista et al., 2017, among others) was  
135 favoured over the alternative use of a total station (Kluskens, 1990; Dibble et al., 1997;  
136 McPherron, 2005; Enloe, 2006; Bernatchez, 2010, among others), mostly due to the  
137 time-restricted conditions of the rescue excavation conducted at Marathousa 1.

138 Measurements of the bearing (azimuth) and plunge (dip) of elongated finds were  
139 taken along the symmetrical longitudinal a-axis (SLA) of bones (Domínguez-Rodrigo  
140 and García-Pérez, 2013), lithic artefacts (Bertran and Texier, 1995) and wood frag-  
141 ments (Macdonald and Jefferson, 1985), using the lowest endpoint of the a-axis as an  
142 indicator of the vector direction.

143 Other major axes have been alternatively used with the recent application of GIS  
144 techniques to retrieve orientation data from secondary source (i.e., excavation photo-  
145 graphs, drawings or maps) (Boschian and Saccà, 2010; Benito-Calvo and de la Torre,  
146 2011; de la Torre and Benito-Calvo, 2013; Walter and Trauth, 2013; García-Moreno  
147 et al., 2016; Sánchez-Romero et al., 2016). However, the experimental works of Domínguez-  
148 Rodrigo and García-Pérez (2013) and Domínguez-Rodrigo et al. (2014c) showed that  
149 the SLA, defined as the major axis which symmetrically divide the bone, is more accu-  
150 rate in determining the preferential orientation of anisotropic assemblages. This a-axis  
151 is widely used in taphonomic studies (Toots, 1965; Voorhies, 1969; Eberth et al., 2007;  
152 Domínguez-Rodrigo et al., 2012, 2014a; Aramendi et al., 2017, among others) and, as  
153 the artefact major axis (Krumbein, 1941), in studies which employ a sedimentologi-  
154 cal approach to archaeological fabric (Bertran and Texier, 1995; Bertran et al., 1997;  
155 Lenoble and Bertran, 2004; Benito-Calvo et al., 2009, among others).

156 The present study focuses on the excavated stratigraphic units in which most of the  
157 archaeological and palaeontological remains were recovered in both excavation areas,  
158 namely in UA3c and UA4 in Area A, and UB4c and UB5a in Area B. From the total,  
159 subset samples of material were used for each specific spatial analysis. For the fabric  
160 analysis we included material collected until 2016. For the vertical distribution and  
161 point pattern analyses, the region of investigation was limited to the squares excavated  
162 from 2013 until 2015, 25 and 29 square meters respectively in each area.

163 The analyses were performed in R statistical software (R Core Team, 2017). In  
164 order to make this research reproducible (Marwick, 2017; Marwick et al., 2017), a  
165 repository containing a compendium of data, source code and text is open licensed and  
166 available at the DOI: [10.5281/zenodo.822273](https://doi.org/10.5281/zenodo.822273)

### 167 2.1. Fabric analysis

168 The taphonomic study of the orientation pattern of elongated sedimentary particles,  
169 including bones and artefacts, first addressed by Voorhies (1969); Isaac (1967); Bar-  
170 Yosef and Tchernov (1972); Schick (1986), more recently led to a noteworthy develop-  
171 ment of methods and propagation of applications in Palaeolithic site formation studies  
172 (Bertran and Texier, 1995; Bertran et al., 1997; Lenoble and Bertran, 2004; Lenoble  
173 et al., 2008; McPherron, 2005; Benito-Calvo et al., 2009, 2011; Benito-Calvo and de la  
174 Torre, 2011; Bernatchez, 2010; Boschian and Saccà, 2010; Domínguez-Rodrigo et al.,  
175 2012; Domínguez-Rodrigo and García-Pérez, 2013; Domínguez-Rodrigo et al., 2014c;  
176 de la Torre and Benito-Calvo, 2013; Walter and Trauth, 2013; García-Moreno et al.,  
177 2016; Sánchez-Romero et al., 2016, among others).

178 Fabric analysis can provide valuable insight into site formation and taphonomic  
179 processes, allowing discrimination between different orientation patterns (isotropic,  
180 linear or planar) associated with a range of sedimentary processes. Whereas water-flow  
181 deposits are generally characterized by relatively good sorting and preferred orientation  
182 of clasts parallel, or normal to the flow direction (linear fabric) (Petruglia and Potts,  
183 1994); debris-flow deposits mostly exhibit massive, poorly bedded mixtures of un-  
184 sorted sediments and random orientation of clasts (isotropic fabric), except at the flow  
185 margins where linear fabric may occur (Pierson, 2005). On the other hand, undisturbed  
186 archaeological sites, as well as experimental sites, have been observed to have planar  
187 fabric (Bertran et al., 1997; Lenoble and Bertran, 2004). Nevertheless, grey zones exist

188 between depositional processes, so that an unequivocal discrimination based only on  
189 fabric observations is often not possible, and other taphonomic criteria must also be  
190 considered (Lenoble and Bertran, 2004). As an example, while overland flows (runoff)  
191 have been observed to show planar fabrics (Lenoble and Bertran, 2004), anisotropy  
192 without significant transport can be caused in a lacustrine floodplain by low-energy pro-  
193 cesses such as lake transgression and regression, as well as water-sheet flows formed  
194 during rainy seasons (Cobo-Sánchez et al., 2014).

195 At the margin of a lacustrine environment, relatively close to the surrounding re-  
196 lief, a combination of high- and low-energy processes can be expected. According to  
197 the sedimentological and micromorphological study of the Marathousa 1 site, mud-  
198 flows and hyperconcentrated flows are associated with the main find-bearing horizons  
199 (Karkanas et al., this issue). Hyperconcentrated flows are intermediate states, defined  
200 by sediment concentration, in the continuum between subaerial water flows and debris  
201 flows. Benvenuti and Martini (2002) reported that, when a turbulent hyperconcentrated  
202 flow expands over a surface - as in the case of Marathousa 1 - a two-phase flow may  
203 develop, with a more concentrated, coarser grained bottom flow-layer (traction carpet)  
204 moving slower than the upper turbulent flow-layer carrying washload and suspended  
205 load. Resultant deposit may exhibit diagnostic inverse grading, or a continuously ag-  
206 grading bed. Parallel or normal orientation of the clast to the flow direction can be  
207 observed (Benvenuti and Martini, 2002). Moreover, a simulation model showed that  
208 linear fabric can develop in mudflows as well. However, after deposition, settling of the  
209 clasts may affect the fabric to some extent, depending on the viscosity of the mudflow  
210 (Lindsay, 1968).

211 As part of our three-prong spatial analytic approach, we conducted comparative  
212 fabric analysis with the aim to investigate the dynamics of the depositional processes  
213 at Marathousa 1.

214 Since fabric strength has been found to be positively correlated with the shape and  
215 size of the clast, for the fabric analysis we subset samples of remains with length  $\geq$  2 cm  
216 and elongation index (the ratio length/width)  $I_e \geq 1.6$  (Lenoble and Bertran, 2004). The  
217 samples are listed in Table 1 and include mostly wood fragments and faunal remains  
218 from the four stratigraphic units under investigation. Bones have been found to readily  
219 react to water flow and show very early anisotropic patterns (Domínguez-Rodrigo et al.,  
220 2014c). Flume experiments showed that wood fragments as well tend to align parallel  
221 to the current direction (Macdonald and Jefferson, 1985). No distinction of skeletal  
222 elements was made, both due to the high fragmentation rate of faunal remains in Area  
223 B, and because recent experiments showed a similar orientation pattern for different  
224 bone shapes (Domínguez-Rodrigo et al., 2012; Domínguez-Rodrigo and García-Pérez,  
225 2013).

226 The sample of bones belonging to the individual of *Elephas (P.) antiquus* from  
227 Area A was analysed separately and included the humerus, ulna, femur and tibia; the  
228 atlas, axis and 16 complete vertebrae or vertebral fragments; 29 complete ribs or rib  
229 fragments; 2 calcanea; 4 metatarsals/metacarpals; the pyramidal; the trapezoid and the  
230 pelvis. The sample from UB5a was too small (only 7 observations) and was there-  
231 fore excluded. In order to asses the reliability of the orientation data recorded using  
232 the clock method, we separately analysed two sub-samples from unit UB4c, selected  
233 from a set of finds recorded using both methods. All the sampled observations are

Table 1: List of sampled observations for the fabric analysis.

| Sample                  | <i>n</i> | Type  |      |        |
|-------------------------|----------|-------|------|--------|
|                         |          | Fauna | Wood | Lithic |
| UA3c                    | 49       | 23    | 25   | 1      |
| UA4                     | 38       | 8     | 30   | -      |
| <i>E. (P.) antiquus</i> | 63       |       |      |        |
| UB4c                    | 38       | 30    | 1    | 7      |

representative of the whole study area.

Rose diagrams and uniformity tests, such as Rayleigh, Kuiper, Watson and Rao tests (Jammalamadaka et al., 2001), were used to visualise and evaluate circular isotropy in the sample distribution. The Rayleigh test is used to assess the significance of the sample mean resultant length ( $\bar{R}$ ), assuming that the distribution is unimodal and not bi- or plurimodal. The  $\bar{R}$  ranges from 0 to 1: values close to 1 indicate that the data are closely clustered around the mean direction; when the data are evenly spread  $\bar{R}$  has a value close to 0. A  $p$  – value lower than 0.05 rejects the hypothesis of uniformity with a 95% confidence interval. Kuiper, Watson and Rao are omnibus tests used to detect multimodal departures from circular uniformity. The Watson's goodness of fit test was conducted for the von Mises distribution (circular normal distribution). The test results are evaluated against critical values: a result higher than the critical value rejects with confidence the null hypothesis.

Randomness testing of three-dimensional data was conducted with the Woodcock  $S_1/S_3$  test (Woodcock and Naylor, 1983). Considering both the plunge and bearing of the oriented items, this method, based on three ordered eigenvalues ( $S_1, S_2, S_3$ ), is able to discriminate the shape and strength of the distributions. The shape parameter  $K = \frac{\ln(S_1/S_2)}{\ln(S_2/S_3)}$  ranges from zero (uni-axial girdles) to infinite (uni-axial clusters). The parameter  $C = \ln(S_1/S_3)$  expresses the strength of the preferential orientation, and its significance is evaluated against critical values from simulated random samples of different sizes. A perfect random uniform distribution would have  $C = 0$  and  $K = 1$ .

The Benn diagram (Benn, 1994) adds to the Woodcock test an isotropy ( $IS = S_3/S_1$ ) and an elongation ( $ES = 1 - (S_2/S_1)$ ) index. Like the former method, it is able to differentiate between linear (cluster), planar (girdle) or isotropic distributions. There are no published raw data from actualistic studies on hyperconcentrated flows or other depositional processes affecting the orientation of bones and artefacts deposited on lacustrine floodplains (but see Morton (2004) and Cobo-Sánchez et al. (2014) as pioneer studies on this subject). However, we included in the Benn diagram references to published results from observation of fabrics in modern subaerial slope deposits, i.e., debris flow and runoff (Bertran et al., 1997; Lenoble and Bertran, 2004).

## 2.2. Vertical distribution

The vertical distribution of materials has been long investigated with the aim of identifying cultural levels, by visually interpreting cross-sectional plots. However, recent advances in GIS techniques allow to inspect at higher resolution the three-dimensional distributions of archaeological remains (McPherron et al., 2005; Anderson and Burke, 2008, among others).

Table 2: List of sampled observations for the vertical distribution and point pattern analyses.

| Sample | <i>n</i> | Lithic class |       |            |      |      | Faunal class |      |       |            |
|--------|----------|--------------|-------|------------|------|------|--------------|------|-------|------------|
|        |          | Debris/chip  | Flake | Bone flake | Tool | Core | Indet.       | Bone | Tooth | Microfauna |
| UA3c   | 279      | 46           | 2     | -          | 1    | -    | 1            | 171  | 14    | 44         |
| UA4    | 61       | 3            | 1     | -          | -    | -    | -            | 45   | 4     | 8          |
| UB4c   | 1243     | 753          | 154   | 1          | 34   | 6    | 2            | 246  | 28    | 19         |
| UB5a   | 101      | 50           | 12    | -          | 3    | -    | -            | 30   | 3     | 3          |

270 In analysing the vertical dispersion of material at Marathousa 1, we provisionally  
 271 assume that a general concentration of unsorted lithic artefacts and faunal remains in  
 272 the proximity of the erosional surfaces would support an autochthonous origin of the  
 273 assemblages; whereas a homogeneous vertical distribution of remains from the UA3c  
 274 and UB4c units would suggest an allochthonous origin, significant transport and sub-  
 275 sequent redeposition of the material. Indeed, massive process such as mudflows or hy-  
 276 perconcentrated flows, have high erosional power and rather chaotic structure, which  
 277 may result in inverse or normal grading (Benvenuti and Martini, 2002).

278 In order to estimate the degree of vertical dispersion while controlling for the size  
 279 of the archaeological material, dimensional classes were set up following typological  
 280 criteria. Lithic artefacts were classified as debris/chips when smaller than a cutoff  
 281 length of 15 mm (Tourloukis et al., this issue). Other classes include flakes, tools and  
 282 cores; the latter being the bigger and heavier debitage product. Table 2 summarises  
 283 the sample size for each class. Lithic debris/chips constitute the larger part of the  
 284 assemblage from UB4c (60%) and UB5a (49%); whereas in Area A they represent  
 285 only a moderate percentage in the upper UA3c unit (16%). The very rare presence of  
 286 lithic artefacts in the underlying unit UA4 is nevertheless significant. In this unit, the  
 287 faunal remains are also found in much lower numbers, their number reduced to one  
 288 fourth of those found in UA3c. For the point pattern analysis (see below), we used the  
 289 same subset of material for both excavation areas.

290 For Area B, the material recovered from the water-screening was randomly prove-  
 291 nanced according to the 5 cm depth of the excavated spit and the coordinates of the  
 292 50x50 cm quadrant of the excavation square. Following the same excavation protocol,  
 293 the same procedure was applied for the water-screened material of Area A, which was  
 294 randomly provenanced according to 3D-coordinates of the 1x1 m excavation square  
 295 and 10 cm spit.

296 Ordinary Kriging interpolation of the recorded points of contact between the UA3c/UA4  
 297 and the UB4c/UB5a stratigraphic units were used to reconstruct the UA3c/4 and UB4c/5a  
 298 erosional surfaces (Fig. 5a,b). In geostatistics, Kriging is a method of interpolation  
 299 which, from a modelled function of spatial autocorrelation between known points (e.g.,  
 300 recorded elevations), calculates values of unknown points (e.g., predicted elevations).  
 301 Thus, in order to address our specific objective, i.e., to quantify and analyse the vertical  
 302 distribution of the archaeological and palaeontological material, we measured the min-  
 303 imum orthogonal distance (*d*) of each specimen to the interpolated erosional surface  
 304 (Fig. 5c). For the units above and below this surface (i.e., UB4c and UB5a), the rela-  
 305 tive distribution of lithic classes and faunal remains was informally tested by means of  
 306 kernel density estimations.

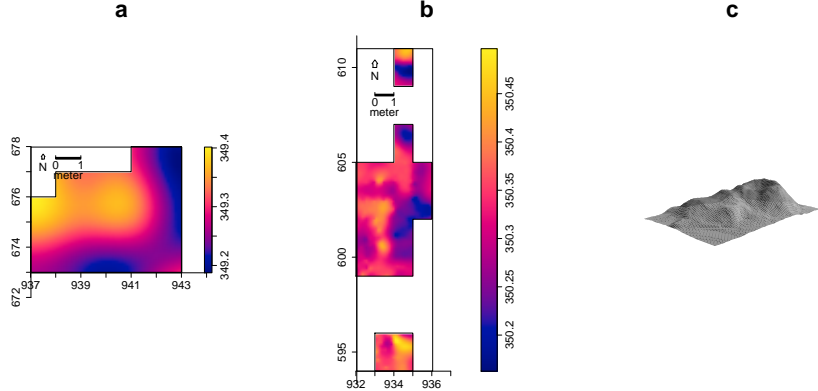


Figure 5: Ordinary Kriging interpolation of the UA3c/4 (a) and UB4c/5a (b) erosional surface; the color scale denotes elevation a.s.l. Illustration of the method used to quantify the vertical dispersion of remains with respect to the UA3c/4 (a) and UB4c/5a (b) surface.

Contrary to Area B, in Area A the UA3c/4 erosinal contact is rather mixed than sharp: parts of the eroded unit UA4 are mixed with pockets of the UA3c organic-rich silty sands and intraclast-rich mudflows (Karkanas et al., this issue). However, from sparse known points of the erosional contact, the UA3c/4 surface was interpolated and the vertical dispersion of remains estimated as well. The elephant remains were excluded from this analysis, since they clearly lie horizontally at the UA3c/4 contact (Fig. 4a and SI).

Finally, a Student's two sample t-test allowed us to compare the empirical distributions of different groups of remains for each stratigraphic unit.

### 2.3. Point pattern analysis

A spatial point pattern is defined as the outcome of a random spatial point process (repetitions of it would always create a different pattern). The observed patterns of the archaeological and palaeontological remains were treated as manifestations of spatial point processes, i.e., site formation processes. Point pattern analysis investigates the spatial arrangement of points with the aim of identifying spatial trends. In order to integrate the previous studies of the fabric and vertical distributions, we directed our point pattern analysis equally to the intensity of the patterns (the rate of occurrence of the recorded finds) and to the spatial interaction between different types of finds.

As the average number of random points per unit area, intensity informs about homogeneity or inhomogeneity in the distribution of events (e.g., clasts) generated by a point process (e.g., mudflow), i.e., whether the rate of occurrence is uniform or spatially varying across the study area. Intensity, usually non-parametrically evaluated by means of kernel density estimation (Diggle, 1985), was assessed for the distribution of material from the UB4c, UB5a and UA3c units. Cross-validation bandwidth, which

331 assumes a Cox process, and edge correction were applied using the methods described  
332 in [Diggle \(1985\)](#).

333 In the presence of a covariate, it is recommended to further investigate the dependence  
334 of intensity on that explanatory variable ([Baddeley et al., 2012](#)). In order to  
335 evaluate whether variation in the density of materials was correlated to the topography  
336 of the erosional surface, we computed a local likelihood smoothing estimate of the in-  
337 tensity of remains from UB4c as a function of the UB4c/5a surface elevation model.  
338 Formal tests enabled us to assess the evidence of that dependence and to quantify the  
339 strength of the covariate. The Kolmogorov-Smirnov test of CSR (Complete Spatial  
340 Randomness) and Berman's  $Z_2$  statistics were used to test the strength of evidence for  
341 a covariate effect. The Receiver Operating Characteristic (ROC) plot, and the area  
342 under the ROC curve (AUC), closely related to Berman's  $Z_2$  test, measure the magni-  
343 tude of the covariate effect. AUC values close to 1 or 0 indicate strong discrimination,  
344 whereas intermediate values (0.5) suggest no discrimination power.

345 Intensity, evaluated by means of kernel density maps, although informative and  
346 widespread in the literature, nonetheless does not provide sufficient information to re-  
347 liably infer about site formation processes.

348 Whereas intensity is a first-order property of the point process, multiscale inter-  
349 point interaction is measured by second or higher-order moment quantities, such as the  
350 Ripley's  $K$  correlation function ([Ripley, 1976, 1977](#)) and the distance  $G$ -,  $F$ - and  $J$ -  
351 functions. Three different types of inter-point interaction are possible: random, regular  
352 or cluster. In a hypothesis-testing framework, pointwise envelopes are computed by  
353 a number of random simulations of the null hypothesis (i.e., random/Poisson distribu-  
354 tion). Thus, values of the empirical distribution (black solid line) are plotted against  
355 the benchmark value (red dotted line) and the envelopes (grey area) which specify the  
356 critical points for a Monte Carlo test ([Ripley, 1981](#)). Regular patterns are assumed to  
357 be the result of inhibition processes, while cluster patterns are the result of attraction  
358 processes.

359 In order to test the spatial interaction between remains associated with the erosional  
360 event of UB4c and those associated with the underlying UB5a unit, we treated the data  
361 as a multivariate point pattern, assuming that the point patterns in UB4c and UB5a are  
362 expressions of two different stationary point processes, i.e., depositional events. We  
363 performed a cross-type pair correlation function ( $g_{ij}(r)$ ), derivative of the multitype  
364  $K_{ij}(r)$  function, which is the expected number of points of type  $j$  lying at a distance  
365  $r$  of a typical point of type  $i$ . The function is a multiscale measurement of the spatial  
366 dependence between types  $i$  (UB4c) and  $j$  (UB5a). Randomly shifting in 199 Monte  
367 Carlo permutations each of the two patterns, independently of each other, estimated  
368 values of  $\hat{g}_{ij}(r)$  are compared to a benchmark value  $g_{ij}(r) = 1$ , which is consistent with  
369 independence or at least with lack of correlation between the two point processes.

370 In addition to the pair correlation function, the multitype nearest-neighbour  $G_{ij}(r)$   
371 function was used to estimate the cumulative distribution of the distance from a point of  
372 type  $i$  (UB4c) to the nearest point of type  $j$  (UB5a). It measures the spatial association  
373 between the two assemblages. For the cross-type  $G$ -function, the null hypothesis states  
374 that the points of type  $j$  follow a Poisson (random) distribution in addition to being  
375 independent of the points of type  $i$ .

376 Thus, in a randomisation technique, when the solid line of the observed distribution

( $\hat{G}_{ij}(r)$  or  $\hat{g}_{ij}$ ) is above or below the shaded grey area, the pattern is significantly consistent with clustering or segregation, respectively. In order to reduce the edge effect bias in estimating the correlation between points, we implemented Ripley's isotropic edge correction (Ohsen, 1983; Ripley, 1988).

Complete spatial randomness and independence (CSRI) of the two point processes (UB4c and UB5a) would support an allochthonous origin hypothesis for the assemblage recovered from the UB4c unit. According to the allochthonous model, the massive, chaotic UB4c flow event randomly re-elaborated the material embedded in it, independently from the material deposited in UB5a. On the other hand, positive or negative association can be interpreted as expressions of different autochthonous processes.

Similarly, the particle size horizontal distribution of the lithic assemblage from UB4c was investigated by means of a transformation of the multitype  $K$ -function ( $K_{i\bullet}(r) - K(r)$ , see Baddeley et al. (2015), p.608). In this case, we treated the data as the manifestation of a single multitype point process. In a joint distribution analysis, the locations and types of points are assumed to be generated at the same time. The null model of a random labelling test states that the type of each point is determined at random, independently of other points, with fixed probabilities. The multitype  $K$ -function was estimated for a subset of possible combinations of coupled classes of remains, and evaluated against the envelope of 199 Monte Carlo permutations.

Whereas the null hypothesis of randomness is consistent with an allochthonous model, spatial clustering or segregation would support an autochthonous model. Specifically, the close occurrence of small specimens, such as lithic debris/chips, with larger dimensional classes of remains would suggest the lack of sorting by natural depositional processes predating the UB4c flow event (when the UB5a surface was exposed). On the other hand, spatial segregation would suggest the action of sorting processes, such as winnowing.

As for the three-dimensional distribution of the lithic artefacts in Area A, and their spatial association with the partial skeleton of the *E. (P.) antiquus*, we applied three-dimensional univariate and bivariate second-order functions. A rectangular box of 20 square meters and 80 cm vertical extent was selected for the analyses (green outline in Fig. 11a). Assuming homogeneity, the univariate pair correlation function ( $g_3(r)$ ) was estimated for the pattern of all the artefacts (mostly debris/chips) from UA3c and UA4.

In the specific context of the site, complete spatial randomness (CSR) would suggest that the pattern most probably is the result of a random distribution process, such as a high energy mass movement, thus supporting an allochthonous model of deposition. On the other hand, spatial aggregation would support a primary origin of the assemblage. Nevertheless, topography and natural obstructions may generate spatial clustering as well.

In support to the pair correlation function, the cross-type nearest-neighbour function has been applied in order to compute, for each artefact recovered from the UA3c and UA4 units, the nearest point of the three-dimensional clouds of points associated with the elephant skeleton. A prevalence of short distances would indicate aggregation of the lithic artefacts around the mass of the elephant; whereas a uniform or symmetric distribution would support the action of random independent processes

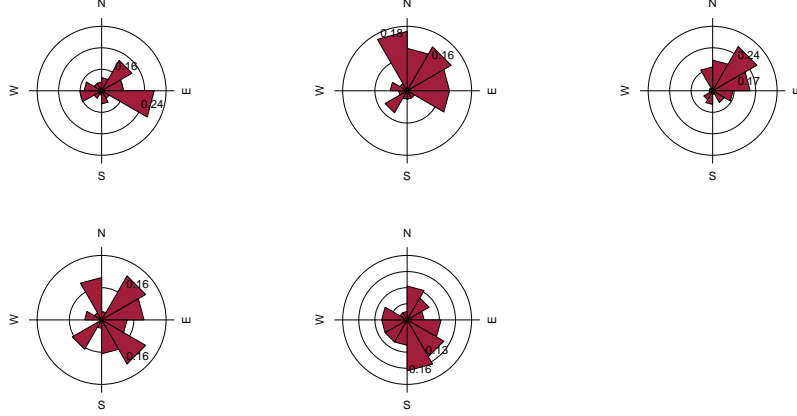


Figure 6: Rose diagrams showing the bearing patterns of samples from UA3c (a), UA4 (b), the elephant carcass (c) and UB4c (d: clock method, e: compass method).

Table 3: Value and  $p$  – value of circular uniformity test statistics.

| Sample                  | mean dir. | Rayleigh  |           | Kuiper |                  | Watson |                  | Rao      |        |
|-------------------------|-----------|-----------|-----------|--------|------------------|--------|------------------|----------|--------|
|                         |           | $\bar{R}$ | $p$       | $V_n$  | $p$              | $U^2$  | $p$              | $U$      | $p$    |
| UA3c                    | 77.17°    | 0.268     | 0.029     | 2.4698 | <0.01            | 0.2967 | <0.01            | 271.8367 | <0.001 |
| UA4                     | 35.79°    | 0.386     | 0.003     | 2.5656 | <0.01            | 0.3437 | <0.01            | 246.3158 | <0.001 |
| <i>E. (P.) antiquus</i> | 54.64°    | 0.489     | 2.775e-07 | 3.4811 | <0.01            | 0.906  | <0.01            | 291.4286 | <0.001 |
| UB4c (clock)            | 91.66°    | 0.276     | 0.054     | 1.8963 | 0.01< $p$ <0.025 | 0.1937 | 0.025< $p$ <0.05 | 255.7895 | <0.001 |
| UB4c (compass)          | 151.17°   | 0.243     | 0.106     | 1.3944 | >0.15            | 0.1268 | >0.10            | 128.5263 | >0.10  |

### 3. Results

#### 3.1. Fabric analysis

The rose diagrams in Fig. 6 visualise the circular distributions of the examined specimens. Overall, the UA4 sample and the sample of elephant bones show unimodal distributions with predominant peaks in the NE quadrant; while the ones from units UA3c and UB4c suggest multimodal distributions. Specifically, the UA4 sample distribution (Fig. 6b) spreads largely in the NE quadrant. Similarly, the circular distribution of the elephant sample (Fig. 6c), mainly lying in UA4, resembles the former distribution: it is skewed to the SW and concentrated in the NE quadrant. On the other hand, the UA3c sample (Fig. 6a) shows a bimodal distribution with two peaks to the E and NE, and the two samples from Area B (Fig. 6d,e) suggest a different multimodal scenario uniformly distributed.

Table 3 summarises the results of the circular uniformity tests. With regard to the UA3c sample, the Rayleigh test ( $p$  – value = 0.03) rejected the null hypothesis of circular uniformity. The mean resultant length ( $\bar{R} = 0.27$ ) and the mean direction of 77° are thus significant, assuming the distribution is unimodal. However, the rose diagram (Fig. 6a) showed a bimodal distribution. The Kuiper, Watson and Rao omnibus tests, more powerful than the Rayleigh test in detecting multimodal deviation from uniformity, also rejected the null hypothesis of uniformity, therefore suggesting significant

441 anisotropy in the distribution.

442 For the UA4 sample and the subset of elephant bones, all the uniformity tests agreed  
443 in rejecting the null hypothesis in favour of a preferentially oriented distribution. The  
444 Elephant sample, with respect to the other, showed significantly higher test results,  
445 thus stronger anisotropy. As suggested by the rose diagrams (Fig. 6c), this sample has  
446 a mean direction towards the NE ( $55^\circ$ ) and relatively low circular variance ( $29^\circ$ ).

447 The UB4c sub-samples had discordant test results when considering the omnibus  
448 statistics. However, according to the Rayleigh test, the mean resultant lengths ( $\bar{R}$ )  
449 and the mean directions were not significant for both sub-samples of measurements:  
450  $p - values > 0.05$  failed to reject the null hypotheses of isotropy with 95% confidence  
451 interval. This result is well confirmed by the Kuiper, Watson and Rao tests for the  
452 sub-sample of measurements recorded using the compass. Conversely, the omnibus  
453 tests failed to reject the hypotheses of uniformity for the other sub-sample of measure-  
454 ments recorded with the clock method. The rose diagram (Fig. 6d) suggested for the  
455 latter distribution strong multimodality, with uniformly spread peaks. The contrasting  
456 results obtained for the UB4c sub-samples are most probably due to the shape of those  
457 distributions. Indeed, the clock system, being less accurate, tends to produce a less  
458 dense distribution, more subject to show a multimodal shape when the distribution is  
459 actually uniform (Fig. 6a,d).

460 The Woodcock eigenvalues ratio graph (Fig. 7a) presents the shape ( $K$ ) and strength  
461 ( $C$ ) of the distributions. Fig. 7b plots confidence levels of Monte-Carlo critical  $C$  val-  
462 ues, varying for sample sizes. The two sub-samples from Area B nearly overlapped,  
463 thus suggesting reliability of the orientation measurements collected using the clock  
464 system, although of low accuracy. The two sub-samples, together with the UA3c sam-  
465 ple, having low  $C$  values, plotted close to the origin of the ratio graph. Therfore, they  
466 indicate weak preferential orientation (UA3c) and significant randomness (UB4c). On  
467 the other hand, the UA4 and the elephant samples, with higher  $C$  values, showed a  
468 stronger and significant tendency to orient preferentially. The shape parameter  $K$  of  
469 the samples varied from  $K = 0.25$  for the UB4c sample measured with the compass,  
470 to  $K = 0.66$  for the one measured with the clock, to  $K = 48$  for the elephant sample.  
471 Overall, all the samples, except the UA3c one ( $K = 1.63$ ), plotted below the average  
472 shape value ( $K = 1$ ) between girdles and clusters distributions.

473 The Benn diagram (Fig. 8) resembles the Woodcock ratio graph (Fig. 7a). The  
474 samples from units UB4c and UA3c clearly plotted at a distance from the UA4 and the  
475 elephant samples. The UB4c samples plotted in the upper corner of the ternary graph,  
476 with the UB4c sub-sample of measurements taken with the compass exhibiting more  
477 isotropy. The UA3c sample, with an elongation index similar to the elephant sample,  
478 but higher isotropix index, plotted towards the centre. Compared to the ranges of fab-  
479 rics recorded for modern natural processes (debris flow, runoff), the fabric from the  
480 UA3c and UB4c units plotted well inside the cluster of debris flows, with the UB4c  
481 (comp) sample suggesting even more random orientations. On the other hand, the  
482 sample of elephant remains, which lie mostly on UA4 and are covered by UA3c, plot-  
483 ted significantly close to the sample from unit UA4. They both presented the lowest  
484 isotropy index ( $IS$ ), but not high elongation index ( $EL$ ). Thus, they plotted in the  
485 average between linear and planar orientations, at the margins of the range of runoff  
486 processes. Yet they still plotted within the cluster of debris flows fabrics. Moreover,

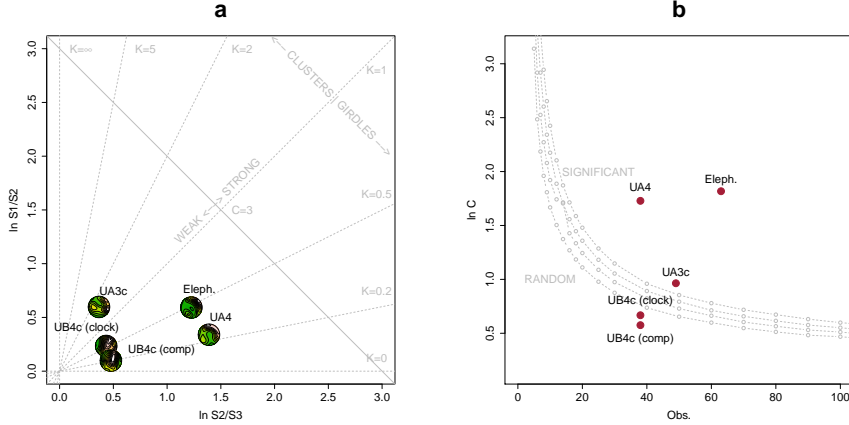


Figure 7: Woodcock's eigenvalues ratio graph (a) and plot of the Monte-Carlo critical  $S_1/S_3$  test values, for varying sample sizes and confidence levels (b), modified from [Woodcock and Naylor \(1983\)](#).

as suggested also by the uniformity tests (Tab. 3), the elephant sample showed a more linear attitude with respect to the UA4 sample.

### 3.2. Vertical distribution

Fig. 9 compares the vertical distribution of the finds from units UA3c and UA4, by means of empirical density functions of the minimum distances ( $d$ ) from each specimen to the UA3c/4 erosional contact (Fig. 5a). Three lithic artefacts (two flakes and one tool) from the UA3c unit, not included in Fig. 9, plotted within 15 cm from the interpolated surface. Only one flake has been found in the lower UA4, at about 17 cm from the UA3c/4 contact, together with three chips. Despite the scarcity of debitage products in this area, waste products (debris/chip) are relatively well represented (16% of the UA3c sample). Their vertical dispersion approximated a normal distribution ( $\mu = 0.24$ ,  $\sigma = 0.15$ ): the Kolmogorov-Smirnov and Shapiro tests failed to rejected the null hypothesis of normality ( $p - value = 0.83$  and 0.075, respectively). Notably, the distributions of the faunal remains from the same unit UA3c were all right skewed, with means ( $\mu$ ) about 20 cm above the UA3c/4 contact. Nevertheless, the Welch two sample t-test ( $p - value = 0.61$ ) failed to reject the null hypothesis that the lithic and faunal sample means are equal. The total distribution of remains from unit UA3c showed a unimodal distribution, skewed to the right, with mode in the proximity of the UA3c/4 surface. Similarly, the vertical distribution of faunal remains recovered from unit UA4 concentrate in the first 10 cm below surface. The density functions altogether clearly confirmed one of the main observations assessed during excavation, namely that, with the elephant remains lying at the UA3c/4 contact and covered by unit UA3c, most of the faunal and lithic material were recovered from unit UA3c and predominantly in the proximity of the UA3c/4 contact.

Fig. 10 shows the empirical density functions of the minimum distances from each specimen from Area B to the UB4c/5a erosional contact (Fig. 5b). The combined

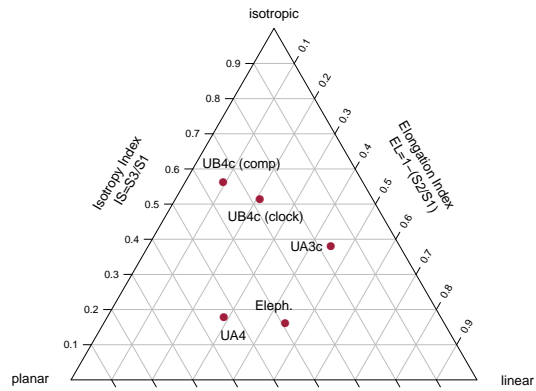


Figure 8: Benn's diagram. Fabric ranges of natural processes modified from Bertran et al. (1997); Lenoble and Bertran (2004).

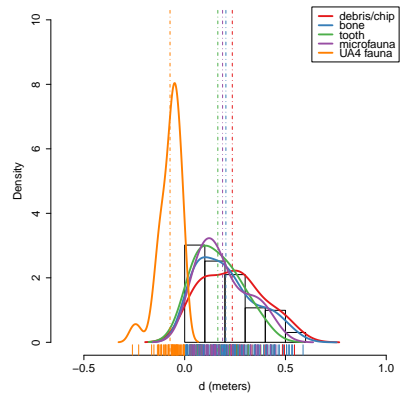


Figure 9: Empirical density functions of minimum orthogonal distances ( $d$ ) to the UA3c/4 surface. The histogram represents the total distribution of remains from UA3c; dashed lines indicate mean values.

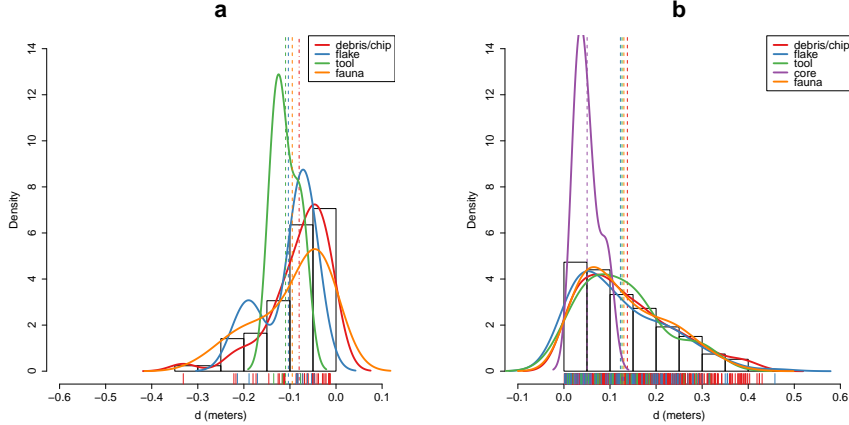


Figure 10: Empirical density functions of minimum orthogonal distances ( $d$ ) to the UB4c/5a surface. The histogram represents the total distribution of remains from UB5a (a) and UB4c (b); dashed lines indicate mean values.

513 distribution of any type of find from the UB5a unit (Fig. 10a) skewed to the left with  
 514 a short tail (up to -0.3 m). The mode, between 5 and 10 cm below the roof of UB5a,  
 515 indicates a general concentration of material very close to the contact of this unit with  
 516 the overlying UB4c, in accordance with the mean distribution of the different classes of  
 517 remains. Although the majority of both the lithic and faunal assemblages were found  
 518 in the uppermost 15 cm of UB5a, few debris/chips and bone fragments occur lower  
 519 in the sequence, yet no more than 30 cm below the roof of this unit. Very few flakes,  
 520 three tools and no cores have been found in this unit. As a whole, the lithic assemblage  
 521 from UB5a, mostly composed by debris/chips, is only 7% of the most conspicuous  
 522 assemblage from UB4c.

523 The global distribution of unit UB4c was right skewed (up to almost 0.6 m) and  
 524 centred at about 5 cm above the contact with the underlying unit UB5a (Fig. 10b).  
 525 Almost 30% of the sample fell exactly at the erosional contact that separates UB4c  
 526 from UB5a. The density estimations of the lithic debris/chip, flakes, tools and faunal  
 527 remains significantly overlap, whereas the distribution of the six cores shows a bimodal  
 528 shape with peaks at 5 and 20 cm above the contact. However, the Welch Two Sample t-  
 529 test of the lithic and faunal sample means failed to reject the null hypothesis ( $p-value =$   
 530 0.6295).

### 531 3.3. Point pattern analysis

532 Results of the point pattern analysis are complementary to those obtained from the  
 533 analysis of the vertical and fabric distributions.

534 Regarding Area A, kernel density estimation and three-dimensional functions were  
 535 applied in order to quantitatively depict the spatial distribution of the lithic assemblage  
 536 in relation to the elephant skeleton.

537 Fig. 11a shows the smoothing kernel intensity estimation of the faunal assemblage  
538 from the UA3c unit. Contour lines delimit the density of the lithic sample. The partial  
539 skeleton of the *E. (P.) antiquus* is superimposed on it. A preliminary visual examination  
540 of the plot suggests a homogeneous distribution of lithics (mostly debris/chips) and  
541 fossils. Spots of higher density appear to be spread around and in association with the  
542 elephant remains.

543 The univariate pair correlation function of the joined lithic assemblage from the  
544 UA3c and UA4 units (Fig. 11b) suggests aggregation of finds. The estimated  $\hat{g}_3(r)$   
545 function (black solid line) wanders above the benchmark value (red dotted line) until  
546 values of  $r = 0.8$ . However, for distances between 35 and 65 cm, it lies above the  
547 grey envelope of significance for the null hypothesis of CSR, indicating that at those  
548 distances artefacts occur significantly closer than expected in the case of random pro-  
549 cesses. For values of  $r > 0.8$ , the function stabilises at values close to 0, suggesting  
550 a Poisson distribution. The plot illustrates the random distribution of finds between  
551 patches of clusters that we observe in Fig. 11a.

552 The histogram in Fig. 11c shows the density of the distances calculated from each  
553 artefact to the nearest-neighbour elephant remain. A right skewed distribution, with a  
554 prevalent peak at 10 cm and mean ( $\mu$ ) 30 cm is an indication of the relatively strong  
555 aggregation of events around the mass of the elephant skeleton.

556 As for Area B, the analysis first focused on the spatial distribution and cross-  
557 correlation of the assemblages from UB4c and UB5a (Fig. 12); and secondly on the  
558 interaction between classes of remains from UB4c (Fig. 13).

559 Figs. 12a,b respectively show kernel density estimations of the combined lithic and  
560 faunal assemblages from both the units analysed. Despite the samples size difference,  
561 a first visual examination suggests the presence of interesting spatial structures.

562 Regarding the UB4c unit (Fig. 12a), the high density of material concentrated  
563 around the western square 934/600 suggests that the pattern could have been the re-  
564 sult of an inhomogeneous, non-uniform depositional process. Visual comparison of  
565 the density plot with the elevation model of the erosional contact between the UB4c  
566 and UB5a units (Fig. 5b) suggests positive correlation between lower elevations (topo-  
567 graphic depressions) and higher density of remains. Fig. 12c shows the results of the  
568  $\rho$ -function, which estimates the intensity of the UB4c sample assemblage as a func-  
569 tion of the covariate underlying topography created by the erosional event. Within the  
570 range of elevation between 350.2 and 350.4 m, the occurrence of finds is higher and  
571 the intensity decreases with the rise of elevation, i.e., finds are more likely to be found  
572 at lower elevations than would be expected if the intensity was constant.

573 Spatial Kolmogorov-Smirnov and Berman's  $Z_2$  (Berman, 1986) statistics were used  
574 in order to test the dependence of the UB4c pattern on the covariate erosional sur-  
575 face. Both KS ( $D = 0.11952$ ,  $p - \text{value} = 7.772e - 16$ ) and  $Z_2$  ( $Z_2 = -7.8447$ ,  
576  $p - \text{value} = 4.34e - 15$ ) significantly rejected the null hypothesis of CSR. Although  
577 the tests suggested evidence that the intensity depends on the covariate, the effect of  
578 the covariate is weak and it seems to have no discriminatory power. The ROC curve  
579 and AUC statistics (0.56), which measure the strength of the covariate effect, suggest  
580 that the underlying UB4c/5a topography does not completely explain the localised high  
581 density of occurrence in the UB4c.

582 Relative spatial segregation seems to occur between the assemblages from UB4c

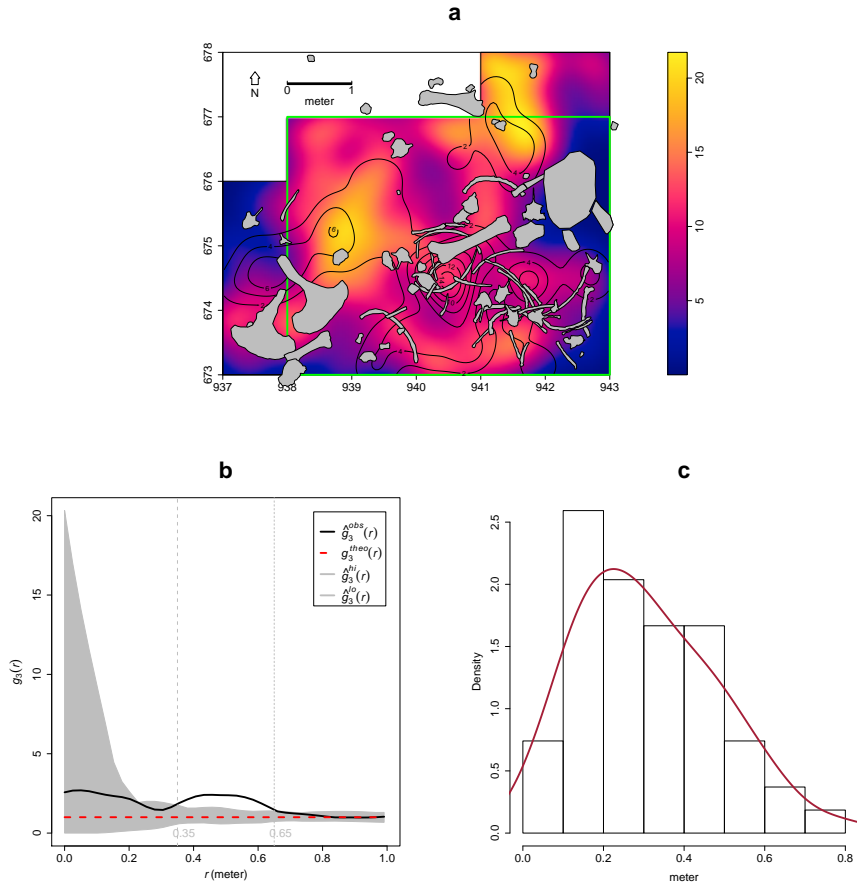


Figure 11: Kernel smoothed intensity function of the faunal assemblages from UA3c. Isolines mark the density of the lithic artefacts from UA3c (a). Pair correlation function ( $g_3(r)$ ) of a three-dimensional pattern of lithic artefacts from UA3c and UA4. Grey envelope of 999 Monte Carlo simulations under the CSR null hypothesis (b). Three-dimensional distance from each lithic artefact from UA3c and UA4 to the nearest neighbour elephant remain (c).

(Fig. 12a) and UB5a (Fig. 12b), with high density of the former distribution corresponding to low density of the latter. The former analysis of the vertical distribution showed that the two assemblages occur very close to their stratigraphic contact. In order to further investigate the spatial interaction between the two depositional events, we applied multitype pair correlation ( $g_{ij}(r)$ ) and nearest-neighbour ( $G_{ij}(r)$ ) functions.

Fig. 12d shows the estimated values of the multivariate  $\hat{g}_{ij}(r)$  function against the envelope of the null hypothesis, obtained by randomly shifting the position of remains from the two distributions in 199 Monte Carlo simulations. For fixed values of  $r$  less than 30 cm the observed function lies below the benchmark value of independence, thus indicating segregation; but it wanders at the lower edge of the grey envelope. For fixed distances of  $r > 0.3$  m the observed and theoretical lines significantly overlap. Overall, the function suggests independence of the two point processes (UB4c and UB5a) at multiple scales.

However, the estimated  $\hat{G}_{ij}(r)$  function (Fig. 12c), running well below the significance grey envelope for fixed values of  $r > 0.3$  m, confirms that the nearest-neighbour distances between remains from UB4c and UB5a are significantly longer than expected in the case of independent processes. Interestingly, at values of  $r < 0.2$  m the observed function failed to reject the null hypothesis of Complete Spatial Randomness and Independence (CSRI).

The particle size spatial distribution of remains from the UB4c unit were investigated by means of a derivative of the multitype  $K$ -function, randomly labelling the classes of remains. Fig.13 shows a selection of the array of possible combinations between classes. In any panel, the estimated function wanders above the benchmark value. Such positive deviations from the null hypotheses suggest that debris/chips are more likely to be found close to the other class of remains than would be expected in case of a completely random distribution. Permutating the lithic debris/chips with flakes (Fig.13a), tools (Fig.13b), cores (Fig.13c) and faunal remains (Fig.13d), the Monte Carlo test results would have been significantly consistent with clustering, if we had chosen distance values  $r > 0.4$ ,  $r > 0.4$ ,  $r > 0.9$ ,  $r > 0.8$ , respectively. Conversely, we could not reject the null hypothesis of CSRI for lesser values of  $r$ .

#### 4. Discussion

Recent excavations at the Middle Pleistocene site of Marathousa 1 have unearthed in one of the two investigated areas (Area A) a partial skeleton of a single individual of *Elephas (P.) antiquus*, whose bones are in close anatomical association, and spatially and stratigraphically associated with lithic artefacts and other faunal remains. In Area B, 60 m to the South of Area A, we collected a much higher number of lithic artefacts (Tourloukis et al., this issue), spatially and stratigraphically associated with other faunal remains, including isolated elephant bones, cervids and carnivores among others (Konidaris et al., this issue).

The two areas are stratigraphically correlated, the main fossiliferous layers (UA3c and UB4c) representing a massive depositional process, such as a hyperconcentrated flow that dumped material in a lake margin context (Karkanas et al., this issue).

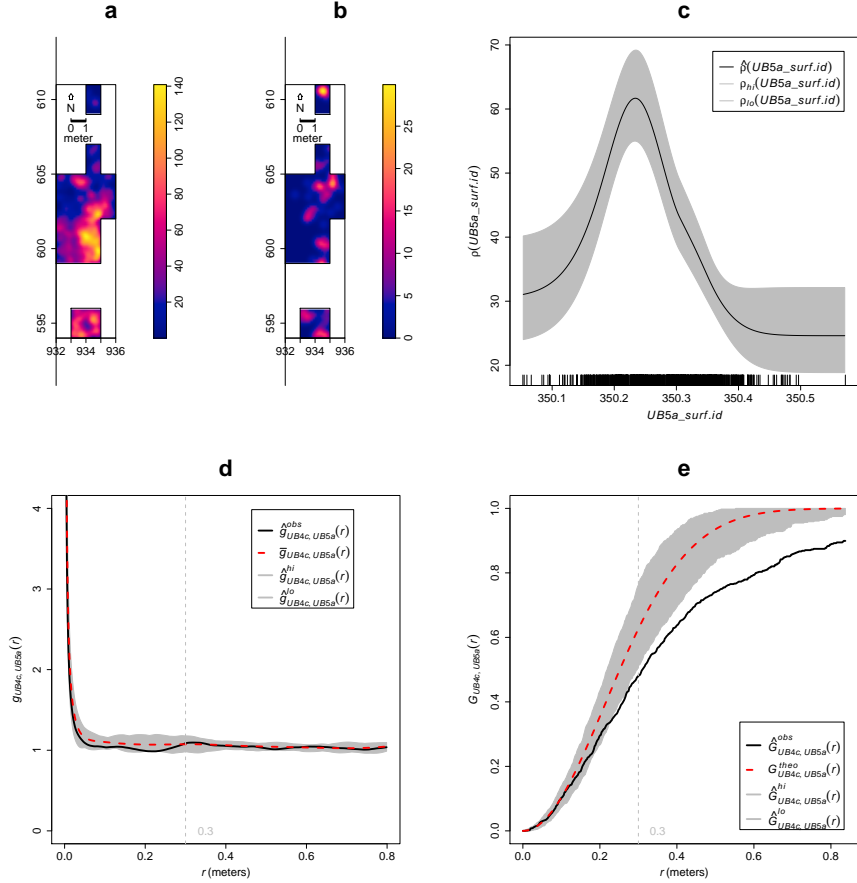


Figure 12: Kernel smoothed intensity function of the lithic and faunal assemblages from UB4c (a) and UB5a (b). Smoothing estimate of the intensity of remains from UB4c, as a function of the erosional surface UB4c/5a. Grey shading is pointwise 95% confidence bands (c). Cross-pattern pair correlation function ( $g_{ij}(r)$ ) between the UB4c and UB5a distributions. Grey envelope of 199 Monte Carlo simulations under the independence of components null hypothesis (d). Multitype nearest-neighbour function ( $G_{ij}(r)$ ) between the UB4c and UB5a distributions (e).

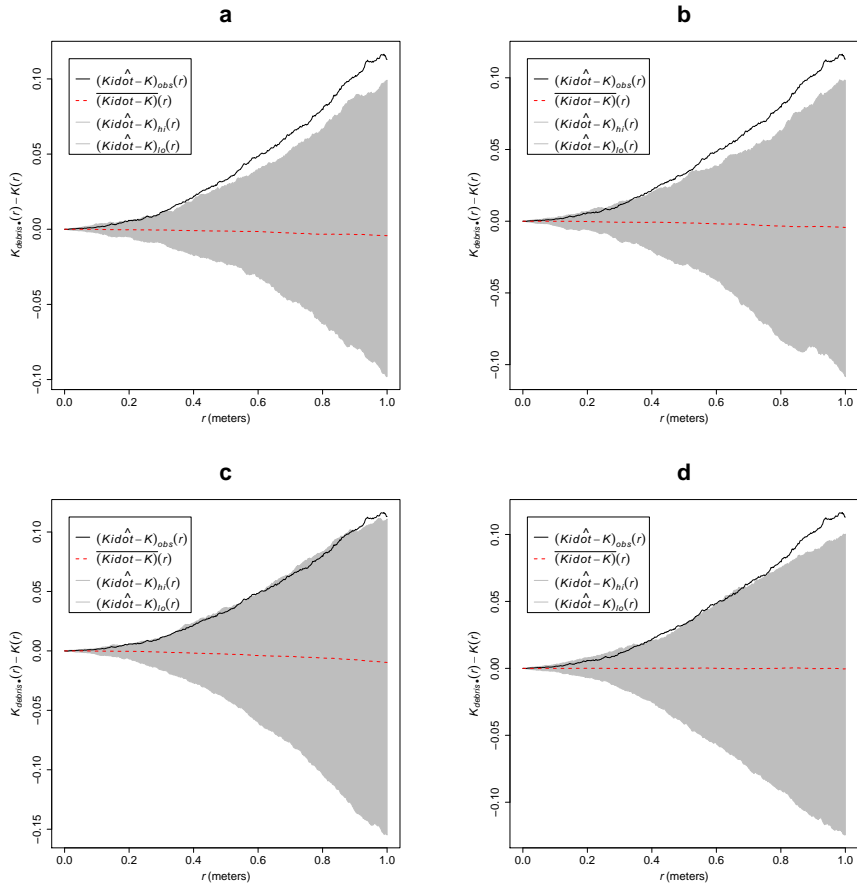


Figure 13: Random labelling test for the UB4c assemblage. Grey pointwise envelope of 199 Monte Carlo permutation of debris/chips with flakes (a); tools (b); cores (c); fossils (d).

625 To date, evidence of butchering (cut-marks) has been identified on two bones of  
626 the elephant skeleton from Area A, as well on elephant and other mammal bones from  
627 Area B (see Konidaris et al. (this issue)).

628 However, due to the secondary depositional nature of the main fossiliferous horizon,  
629 it is of primary importance to evaluate the degree and reliability of the spatial  
630 association of the lithic artefacts with the faunal remains, and especially with the ele-  
631 phant skeleton. In order to tackle our main objective, we applied a comprehensive  
632 set of spatial statistics to the distributions of the archaeological and zooarchaeologi-  
633 cal/palaeontological remains from relevant stratigraphic units of the two areas of in-  
634 vestigation. Preliminary results of our analyses are here discussed for both areas.

#### 635 4.1. Fabric analysis

636 The analysis of the orientation (plunge and bearing) of subsets of remains, mostly  
637 bone, wood fragments and lithic artefacts, showed different patterns for the two main  
638 find-bearing units.

639 The test results (Tab. 3) for the UA4 sample and the sample of elephant remains  
640 - which lie on unit UA4 and are covered by UA3c - indicated significant preferential  
641 orientations towards the NE (Figs. 6b,c). As shown by the Woodcock's (Fig. 7) and the  
642 Benn's diagrams (Fig. 8), these samples plotted together at a distance from the others.  
643 Such convergence suggests that the elephant carcass, the other faunal remains and the  
644 organic material, deposited on unit UA4, were subject to the same processes.

645 Far from the isotropic corner in the Benn's diagram these two samples from Area  
646 A plotted approximately in between the linear and planar extremes, with the elephant  
647 sample showing a more linear fabric. When the results published by Bertran et al.  
648 (1997) and Lenoble and Bertran (2004) from observations of fabrics in modern sub-  
649 aereal slope deposits were used as a reference, the two samples aggregated at the ex-  
650 treme margins of runoff processes. Yet, they still plotted well within the cluster of  
651 debris flows and relatively distant from the linear corner.

652 Although Bertran et al. (1997) studied runoff deposits from different environments  
653 (channel-lag gravels in rills, small gullies, and inter-rill surfaces on alpine slopes; and  
654 faintly laminated gravel lenses on an inactive, small colluvial fan), this result is con-  
655 sistent with the exposure of unit UA4 to overland water-laden processes that occurred  
656 before the flood event UA3c/UB4c. Pockets of thinly bedded organic-rich silty sands  
657 have been found mixed in UA4. These sands in Area A resemble the UB5b/c sandy  
658 deposit in area B, which is associated with relatively high energy fluviale flows entering  
659 the lake margins (Karkanas et al., this issue). Notably, the erosive nature of low-energy  
660 processes triggered by rain-water has been observed on lacustrine floodplains, and  
661 is associated with anisotropic patterns in autochthonous assemblages (Cobo-Sánchez  
662 et al., 2014; Domínguez-Rodrigo et al., 2014c; García-Moreno et al., 2016).

663 Eventually, such relatively high energy flood (UB5b/c) would have had the power  
664 to significantly reorient elements of the elephant carcass and slightly displace them.  
665 However, the elephant skeleton clearly lies on unit UA4 and is covered by UA3c (see  
666 Fig.4 and SI).

667 Unlike bones with a tubular shape (i.e., long bones), ribs and vertebrae are prone  
668 to orient preferentially under high energy processes, less likely under low energy pro-  
669 cesses (Domínguez-Rodrigo and García-Pérez, 2013; Domínguez-Rodrigo et al., 2014c).

670 Interestingly, whereas some of the ribs share the same preferential orientation with the  
671 long bones, others are oriented NW/SE. However, a NW/SE orientation could be con-  
672 sistent with a prevalent NE direction of the flow (and vice-versa), since long bones  
673 could roll orthogonally to the flow direction (Voorhies, 1969). On the other hand, a  
674 higher energy flood would lead to an under-representation of most cancellous grease-  
675 bearing bones, which are prone to be easily transported by water induced processes  
676 (Voorhies, 1969). Yet several carpals, tarsals, metapodials, phalanges, ribs and verte-  
677 brae are present and in close spatial association with the elephant cranium and other  
678 skeletal elements.

679 The presence of many of the skeletal elements suggests that the elephant carcass  
680 was not subjected to high energy processes before the flood event UA3c/UB4c.

681 The fabrics of the UA3c and UB4c samples, with higher isotropix index (*IS*), plotted  
682 at a significant distance from the elephant sample, yet within the cluster of debris  
683 flows (Fig. 8). Indeed, random distribution and orientation of clasts is expected for de-  
684 bris flows, except at flow margins, where preferential orientation and clusters of clasts  
685 have been observed (Pierson, 2005). However, hyperconcentrated flows, such as the  
686 UA3c/UB4c flood event, which fall in between the spectrum of water and debris flows,  
687 may develop parallel or normal orientation to the flow direction (Lindsay, 1968; Ben-  
688 venuti and Martini, 2002). Notably, with respect to the UB4c sample, the UA3c sample  
689 exhibits a higher elongation index (*ES*), similar to that of the elephant sample (Fig. 8).  
690 Rose diagrams (Fig. 6) and uniformity tests (Tab. 3) also suggest similar fabrics of the  
691 samples from Area A.

692 Thus, we can assume that an overland flow, namely UA3c/UB4c, is likely to have  
693 slightly reworked and preferentially oriented to the NE the exposed elements of the  
694 already dismembered (and probably already marginally displaced) elephant carcass,  
695 which mostly preserves close anatomical associations, but not anatomical connections.

696 Although little is currently known about the spatial extension of the UA3c/UB4c  
697 flow event, the different orientation patterns between the two areas could probably  
698 be explained with lateral variability. Indeed, the same event could exhibit different  
699 behaviours at different temporal and spatial points, giving rise to different distribution  
700 patterns.

701 In Area B, two sub-samples from the same stratigraphic unit were analysed, in or-  
702 der to asses the reliability of the orientation data measured with the clock system. Due  
703 to the different shapes of the two distributions (Figs. 6d,e), test statistics reported con-  
704 trasting results (Tab. 3). Indeed, the clock system, recording non-continuous circular  
705 data, tends to produce a distribution more subject to show a multimodal shape when  
706 the distribution is actually uniform. However, the two sub-samples nearly overlapped  
707 when plotted in the three-dimensional Woodcock (Fig. 7) and Benn (Fig. 8) diagrams,  
708 thus suggesting some degree of reliability of the clock method. However, despite mi-  
709 nor differences between the two samples, caution should be paid in analysing grouped  
710 circular data.

#### 711 4.2. Vertical distribution

712 As for the vertical distribution, we assumed that mass processes, such as hypercon-  
713 centrated flows, would predominantly distribute poor to very poor sorted clasts homo-  
714 geneously throughout the sequence (Pierson, 2005). Diagnostic inverse grading, or a

715 continuously aggrading bed can be observed in the resultant deposits ([Benvenuti and](#)  
716 [Martini, 2002](#)). A concentration of unsorted elements in the proximity of the erosional  
717 surface, as well as the absence of any grading, would in turn suggest an autochthonous  
718 assemblage.

719 The lithic assemblage from Area A - the combined units UA3c and UA4 ( $n = 54$ ),  
720 composed by a few debitage products and a relatively high number of debris/chips  
721 and retouch waste products ([Tab. 2](#)) - plotted predominantly in the proximity of the  
722 erosional surface created by the UA3c/UB4c event ([Fig. 5a](#)). The faunal remains from  
723 unit UA3c resemble the distribution of the archaeological assemblage; whereas the  
724 ones from the underlying unit UA4 plotted within 10 cm below the erosional contact  
725 ([Fig. 9](#)). Overall, the material recovered from unit UA3c did not show any grading and  
726 mainly plotted at the bottom of the unit, thus is consistent with the hypothesis of an  
727 autochthonous assemblage.

728 In Area B, two samples from units UB4c ( $n = 1243$ ) and UB5a ( $n = 101$ ) respec-  
729 tively, were analysed ([Tab. 2](#)) for quantifying the minimum orthogonal distance of each  
730 item to the modelled erosional surface ([Fig. 5b](#)).

731 The vertical distribution of lithic artefacts and fossils from unit UB4c showed a pre-  
732 dominant peak right at the contact with the erosional surface. Almost 30% of this rich  
733 sample plotted at a distance between 0 and 5 cm from the erosional contact; whereas  
734 the rest gently skewed to the upper part of the unit, up to about 50 cm. The same distri-  
735 bution was observed for all classes of remains, suggesting no size sorting and an origin  
736 very close to the erosional surface ([Fig. 10b](#)).

737 The density distribution of the sample from the underlying UB5a unit ([Fig. 10a](#))  
738 globally indicates a more constrained vertical displacement of remains (within 30 cm  
739 below the erosional surface). Whereas lithic artefacts and fossils mostly plot right at  
740 the contact and just below it, a few debris/chips and faunal remains were found lower  
741 in the sequence. No size sorting was observed, but, notably, lithic cores are absent and  
742 the debris/chip distribution is wider than the distribution of the few flakes and tools.

743 Field observations of cracks in the clayey UB5a unit testify to shrinking and swelling  
744 during wet and dry cycles ([Karkanas et al., this issue](#)), which suggests that vertical dis-  
745 placement of some small lithics and fossil fragments at lower depths with respect to  
746 the UB5a/4c contact probably resulted from clay desiccation.

747 Likewise, [Lenoble and Bertran \(2004\)](#) documented up to 30 cm vertical dispersion  
748 and frequent vertical plunge of artefacts from the marshy silty clay of the Croix-de-  
749 Canard site, sector 3.

750 Furthermore, a recent experimental study of animal trampling in water saturated  
751 substrates reported negative correlation with artefact size, significant inclination and  
752 greater vertical displacement than any former work: a maximum between 16 and  
753 21 cm, with a mean of about 6 cm ([Eren et al., 2010](#)).

754 The fact that the majority of the remains from units UB4c and UB5a plotted at, or  
755 very close to the contact between these two layers, the relatively high percentage of  
756 lithics in both units, as well as the absence of grading, suggest autochthonous assem-  
757 blages, deposited in UB5a and subsequently eroded *in situ* by the UA3c/UB4c flood  
758 event.

759     4.3. Point pattern analysis

760     The autochthonous hypothesis was further explored by means of point pattern  
761     analysis. According to this model, in both areas the lithic and faunal assemblages  
762     were primarily deposited *in situ* and were subsequently eroded and re-deposited (*sensu*  
763     Fernández-López, 1991) by the hyperconcentrated flow UA3c/UB4c. We assumed  
764     that a completely random spatial distribution of the lithic artefacts and faunal remains  
765     would suggest an allochthonous origin and subsequent re-elaboration (*sensu* Fernández-  
766     López, 1991), with transport to the site by the action of a random massive process.  
767     Nevertheless, clustering of artefacts is not necessarily evidence of human presence.  
768     Aggregation or segregation patterns could be produced by a range of biotic and/or nat-  
769     ural processes. Human activities, topography and physical obstructions alike could  
770     trigger spatial aggregation.

771     The three-dimensional distribution of lithic artefacts from unit UA3c shows signif-  
772     icant clustering for values of  $r$  between 35 and 65 cm. Lithic artefacts occur relatively  
773     close to the skeletal elements of the elephant, at a distance between 20 and 50 cm at  
774     most (Fig. 11). The richest cluster of about 20 lithic artefacts is located to the SW of  
775     the cranium, close to the right femur and the scatter of ribs and vertebrae.

776     Considering the prevalent NE orientation of the elephant bones and the other fau-  
777     nal remains from UA4 and UA3c, it is not unlikely that a SW/NE oriented flood could  
778     have been responsible for the observed accumulation to the SW of the elephant cra-  
779     nium, which would have represented an important obstruction to the flow. A similar  
780     case of clustering of small remains, apparently dammed by a long elephant tusk, has  
781     also been observed at Castel di Guido (Italy) (Boschian and Saccà, 2010). Secondary  
782     deposition by low-energy flows and clustering of artefacts and bones blocked by an  
783     aurochs carcass have been as well documented at the site of 'Ein Qashishadd (Israel)  
784     (Hovers et al., 2014).

785     However, the pair correlation function (Fig. 9b) suggests significant clustering of  
786     lithic artefacts at relatively small scale: a pattern less likely to be produced by a large  
787     scale massive process such as a hyperconcentrated flow. Moreover, clusters of lithic  
788     artefacts occur as well in areas with lower densities of elephant bones.

789     Small scale clustering; proximity to the elephant remains and the erosional sur-  
790     face; absence of spatial size sorting and, on the contrary, the presence of a relatively  
791     high number of lithic debris/chips associated with some flakes, tools and a rich fau-  
792     nal assemblage; close anatomical spatial association of the elephant skeletal elements,  
793     slightly displaced and preferentially oriented: these lines of evidences support the hy-  
794     pothesis of an autochthonous deposition, subject to localised minor reworking.

795     A similar pattern can be observed in Area B, where an initial set of spatial statistics  
796     confirmed that the inhomogeneous density of remains from unit UB4c (Fig. 12a) is  
797     not completely explained by the covariate effect of the underlying complex topography  
798     created by the erosional event UA3c/UB4c (Fig. 5b).

799     Thus, we explored the relative spatial interaction between the UB4c and the un-  
800     derlying UB5a samples. We assumed that complete spatial randomness of the two  
801     independent depositional processes would occur in case of an allochthonous origin and  
802     transportation of the UB4c assemblage. The hypothesis of an autochthonous original  
803     deposition of the faunal and lithic assemblages on the UB5a unit, subsequently eroded

804 *in situ* by a relatively high energy flood (UB4c), was tested by cross-pattern spatial  
805 correlation functions (Figs. 12d,e). Whereas the two samples are vertically adjacent to  
806 the erosional surface (Fig. 10), on the horizontal plane they are both more segregated  
807 than expected for a random distribution.

808 Moreover, for the UB4c sample, an unsorted particle size spatial distribution was  
809 confirmed (Fig. 13). Whereas a random spatial association between dimensional classes  
810 was assumed for an allochthonous model of deposition, the cluster association of small  
811 and large classes of remains suggested that post-depositional processes, such as water  
812 winnowing, have not severely affected the assemblage.

813 Conversely, the extraordinary preservation and number of mint to sharp, unsorted  
814 lithic artefacts from the UB4c unit; their density, positively correlated to the topog-  
815 raphy, and significantly segregated from the underlying distribution of remains; the  
816 vertical proximity of both assemblages from UB4c and UB5a to the erosional surface;  
817 as well as the random orientation pattern of the former, suggest that significant dis-  
818 placement of materials due to the erosional event can be excluded.

819 The faunal and lithic assemblages from unit UB4c therefore most likely derived  
820 from the local erosion of exposed mudflat areas (UB5a layer) and have been slightly  
821 redistributed by the same flood event that capped the elephant in Area A.

822 Further evidence that the recovered assemblage has not undergone substantial re-  
823 working and has retained its original characteristics would come from the refitting anal-  
824 ysis, currently in progress. To date, 4 bone refits have been found in Area B: three from  
825 unit UB4c, respectively at 4.77, 0.05 and 0.01 m distance; and one between two mam-  
826 mal bone fragments from units UB4c and UB5a, at a very short distance (0.09 m).  
827 Interestingly, one of the elements of the most distant refit (a *Dama sp.* mandibular  
828 fragment) shows traces of carnivore gnawing (Konidaris et al., *this issue*).

829 In conclusion, multiple lines of evidence reject an allochthonous hypothesis of de-  
830 position in favour of an authochthonous model. The erosional event UA3c/UB4c repre-  
831 sents an *en masse* depositional process, i.e. a hyperconcentrated flow, in the continuum  
832 between water and debris flow, which would have locally reworked at a small scale  
833 the already exposed or slightly buried and spatially associated lithic and faunal assem-  
834 blages.

835 Although the UA3c/UB4c process represents a snapshot of a relatively short time-  
836 frame, inferences about the use of space by human groups, in terms of knapping  
837 episodes and butchering activities, are unreliable in light of the current information.

838 The spatial pattern observed at the site is indeed the result of the last episode in  
839 a palimpsest of spatial processes. Whereas the erosional event represented by the hy-  
840 perconcentrated flow UA3c/UB4c caps the sequence and preserves the record, little is  
841 known about the eroded underlying occupational horizon.

842 However, whereas hunting or scavenging is still an unsolved matter of debate, con-  
843 sidering the rate of bone fragmentation, the density of lithic debris/chips, the number  
844 of processed bones and their spatial density and association, it is likely that the assem-  
845 blage represents a complex palimpsest of locally repeated events of hunting/scavenging  
846 and exploitation of lake shore resources.

847 More data from high resolution excavations in the coming years will allow us to  
848 refine the coarse-grained spatio-temporal resolution of our inferences about past human  
849 behaviour at Marathousa 1.

850    **5. Conclusions**

851    At the Middle Pleistocene open-air site of Marathousa 1, a partial skeleton of a  
852    single individual of *Elephas (Palaeoloxodon) antiquus* was recovered in stratigraphic  
853    association with a rich and consistent lithic assemblage and other vertebrate remains.  
854    Cut-marks and percussion marks have been identified on the elephant and other mam-  
855    mal bones excavated at the site. The main find-bearing horizon represents a secondary  
856    depositional process in a lake margin context.

857    Understanding the site formation processes is of primary importance in order to  
858    reliably infer hominin exploitation of the elephant carcass and other animals. To meet  
859    this aim, we applied a comprehensive set of multivariate and multiscale spatial analyses  
860    in a taphonomic framework.

861    Results from the fabric, vertical distribution and point pattern analyses are consis-  
862    tent with a relatively high-energy erosional process slightly reworking at a small scale  
863    an exposed (or slightly buried) and consistent scatter of lithic artefacts and faunal re-  
864    mains. These results are in agreement with preliminary taphonomic observations of the  
865    lithic artefacts ([Tourloukis et al., this issue](#)) and the faunal remains ([Konidaris et al.,](#)  
866    [this issue](#)), which also indicate minor weathering and transportation. Our analyses  
867    show that multiple lines of evidence support an autochthonous origin of the lithic and  
868    faunal assemblages, subject to minor post-depositional reworking. Human activities  
869    therefore took place on-site, during an as of yet uncertain range of time.

870    **Acknowledgements**

871    This research is supported by the European Research Council (ERC StG PaGE  
872    283503) awarded to K. Harvati. We are grateful to the Municipality of Megalopolis,  
873    the authorities of the Region of Peloponnese, and the Greek Public Power corporation  
874    (ΔΕΗ) for their support. We also thank Julian Bega and all the participants in the PaGE  
875    survey and excavation campaigns in Megalopolis for their indispensable cooperation.

876    **References**

- 877    Anderson, K. L., Burke, A., 2008. Refining the definition of cultural levels at Karabi  
878    Tamchin: a quantitative approach to vertical intra-site spatial analysis. *Journal of*  
879    *Archaeological Science* 35 (8), 2274–2285.
- 880    Aramendi, J., Uribelarrea, D., Arriaza, M. C., Arráiz, H., Barboni, D., Yravedra, J.,  
881    Ortega, M. C., Gidna, A., Mabulla, A., Baquedano, E., Domínguez-Rodrigo, M.,  
882    2017. The paleoecology and taphonomy of {AMK} (bed i, olduvai gorge) and its  
883    contributions to the understanding of the “zinj” paleolandscape. *Palaeogeography,*  
884    *Palaeoclimatology, Palaeoecology*, –.
- 885    Baddeley, A., Chang, Y.-M., Song, Y., Turner, R., 2012. Nonparametric estimation of  
886    the dependence of a point process on spatial covariates. *Statistics and Its Interface*  
887    5 (2), 221–236.

- 888 Baddeley, A., Rubak, E., Turner, R., 2015. Spatial Point Patterns: Methodology and  
889 Applications with R. Chapman and Hall/CRC, London.
- 890 Bailey, G., 2007. Time perspectives, palimpsests and the archaeology of time. *Journal*  
891 of Anthropological Archaeology 26 (2), 198 – 223.
- 892 Bar-Yosef, O., Tchernov, E., 1972. On the palaeo-ecological history of the site of Ubeidya.  
893 Vol. 35. Israel Academy of Sciences and Humanities, Jerusalem.
- 894 Bargalló, A., Gabucio, M. J., Rivals, F., 2016. Puzzling out a palimpsest: Testing an  
895 interdisciplinary study in level o of abric romaní. *Quaternary International* 417 (Sup-  
896 plement C), 51 – 65, advances in Palimpsest Dissection.
- 897 Benito-Calvo, A., de la Torre, I., 2011. Analysis of orientation patterns in Olduvai  
898 Bed I assemblages using GIS techniques: Implications for site formation processes.  
899 *Journal of Human Evolution* 61 (1), 50 – 60.
- 900 Benito-Calvo, A., Martínez-Moreno, J., Mora, R., Roy, M., Roda, X., 2011. Trampling  
901 experiments at Cova Gran de Santa Linya, Pre-Pyrenees, Spain: their relevance for  
902 archaeological fabrics of the Upper–Middle Paleolithic assemblages. *Journal of Ar-  
903 chaeological Science* 38 (12), 3652–3661.
- 904 Benito-Calvo, A., Martínez-Moreno, J., Pardo, J. F. J., de la Torre, I., Torcal, R. M.,  
905 2009. Sedimentological and archaeological fabrics in Palaeolithic levels of the  
906 South-Eastern Pyrenees: Cova Gran and Roca dels Bous Sites (Lleida, Spain). *Jour-  
907 nal of Archaeological Science* 36 (11), 2566 – 2577.
- 908 Benn, D., 1994. Fabric shape and the interpretation of sedimentary fabric data. *Journal*  
909 of Sedimentary Research 64 (4a), 910–915.
- 910 Benvenuti, M., Martini, I. P., 2002. Analysis of terrestrial hyperconcentrated flows and  
911 their deposit. In: Martini, I. P., Baker, V. R., Garzón, G. (Eds.), *Flood and Megaflood*  
912 *Processes and Deposits*. Vol. 32 of Special Publication of the International Associa-  
913 tion of Sedimentologists. Blackwell Publishing Ltd., pp. 167–193.
- 914 Berman, M., 1986. Testing for spatial association between a point process and another  
915 stochastic process. *Applied Statistics* 35, 54–62.
- 916 Bernatchez, J. A., 2010. Taphonomic implications of orientation of plotted finds from  
917 Pinnacle Point 13B (Mossel Bay, Western Cape Province, South Africa). *Journal of*  
918 *Human Evolution* 59 (3–4), 274 – 288.
- 919 Bertran, P., Hetù, B., Texier, J.-P., Steijn, H. V., 1997. Fabric characteristics of subaerial  
920 slope deposits. *Sedimentology* 44 (1), 1 – 16.
- 921 Bertran, P., Texier, J.-P., 1995. Fabric Analysis: Application to Paleolithic Sites. *Jour-*  
922 *nal of Archaeological Science* 22 (4), 521 – 535.

- 923 Bevan, A., Crema, E., Li, X., Palmisano, A., 2013. Intensities, Interactions, and Un-  
924 certainties: Some New Approaches to Archaeological Distributions. In: Bevan, A.,  
925 Lake, M. (Eds.), Computational Approaches to Archaeological Spaces. Left Coast  
926 Press, Walnut Creek, pp. 27–52.
- 927 Binford, L. R., 1981. Behavioral archaeology and the "pompeii premise". *Journal of*  
928 *Anthropological Research* 37 (3), 195–208.
- 929 Boschian, G., Saccà, D., 2010. Ambiguities in human and elephant interactions? Sto-  
930 ries of bones, sand and water from Castel di Guido (Italy). *Quaternary International*  
931 214 (1–2), 3 – 16.
- 932 Brantingham, P. J., Surovell, T. A., Waguespack, N. M., 2007. Modeling post-  
933 depositional mixing of archaeological deposits. *Journal of Anthropological Archae-*  
934 *ology* 26 (4), 517 – 540.
- 935 Carrer, F., 2015. Interpreting Intra-site Spatial Patterns in Seasonal Contexts: an Eth-  
936 noarchaeological Case Study from the Western Alps. *Journal of Archaeological*  
937 *Method and Theory*, 1–25.
- 938 Cobo-Sánchez, L., Aramendi, J., Domínguez-Rodrigo, M., 2014. Orientation patterns  
939 of wildebeest bones on the lake Masek floodplain (Serengeti, Tanzania) and their  
940 relevance to interpret anisotropy in the Olduvai lacustrine floodplain. *Quaternary*  
941 *International* 322–323 (0), 277 – 284.
- 942 de la Torre, I., Benito-Calvo, A., 2013. Application of GIS methods to retrieve ori-  
943 entation patterns from imagery; a case study from Beds I and II, Olduvai Gorge  
944 (Tanzania). *Journal of Archaeological Science* 40 (5), 2446–2457.
- 945 Dibble, H. L., Chase, P. G., McPherron, S. P., Tuffreau, A., Oct. 1997. Testing the  
946 reality of a "living floor" with archaeological data. *American Antiquity* 62 (4), 629–  
947 651.
- 948 Diggle, P., 1985. A kernel method for smoothing point process data. *Applied Statistics*  
949 (*Journal of the Royal Statistical Society, Series C*) 34, 138–147.
- 950 Domínguez-Rodrigo, M., Bunn, H., Mabulla, A., Baquedano, E., Uribelarrea, D.,  
951 Pérez-González, A., Gidna, A., Yravedra, J., Diez-Martin, F., Egeland, C., Barba,  
952 R., Arriaza, M., Organista, E., Ansón, M., 2014a. On meat eating and human evolu-  
953 tion: A taphonomic analysis of BK4b (Upper Bed II, Olduvai Gorge, Tanzania), and  
954 its bearing on hominin megafaunal consumption. *Quaternary International* 322–323,  
955 129–152.
- 956 Domínguez-Rodrigo, M., Bunn, H., Pickering, T., Mabulla, A., Musiba, C., Baque-  
957 dano, E., Ashley, G., Diez-Martin, F., Santonja, M., Uribelarrea, D., Barba, R.,  
958 Yravedra, J., Barbón, D., Arriaza, C., Gidna, A., 2012. Autochthony and orientation  
959 patterns in Olduvai Bed I: a re-examination of the status of post-depositional biasing  
960 of archaeological assemblages from FLK North (FLKN). *Journal of Archaeological*  
961 *Science* 39 (7), 2116 – 2127.

- 962 Domínguez-Rodrigo, M., Cobo-Sánchez, L., Yravedra, J., Uribelarrea, D., Arriaza, C.,  
963 Organista, E., Baquedano, E., 2017. Fluvial spatial taphonomy: a new method for the  
964 study of post-depositional processes. *Archaeological and Anthropological Sciences*,  
965 1–21.
- 966 Domínguez-Rodrigo, M., Diez-Martín, F., Yravedra, J., Barba, R., Mabulla, A., Baque-  
967 dano, E., Uribelarrea, D., Sánchez, P., Eren, M. I., 2014b. Study of the SHK Main  
968 Site faunal assemblage, Olduvai Gorge, Tanzania: Implications for Bed II tapho-  
969 nomy, paleoecology, and hominin utilization of megafauna. *Quaternary International*  
970 322–323, 153–166.
- 971 Domínguez-Rodrigo, M., García-Pérez, A., 07 2013. Testing the Accuracy of Different  
972 A-Axis Types for Measuring the Orientation of Bones in the Archaeological and  
973 Paleontological Record. *PLoS ONE* 8 (7), e68955.
- 974 Domínguez-Rodrigo, M., Uribelarrea, D., Santonja, M., Bunn, H., García-Pérez, A.,  
975 Pérez-González, A., Panera, J., Rubio-Jara, S., Mabulla, A., Baquedano, E., Yrave-  
976 dra, J., Diez-Martín, F., 2014c. Autochthonous anisotropy of archaeological mate-  
977 rials by the action of water: experimental and archaeological reassessment of the  
978 orientation patterns at the Olduvai sites . *Journal of Archaeological Science* 41 (0),  
979 44 – 68.
- 980 Eberth, D. A., Rogers, R. R., Fiorillo, A. R., 2007. A practical approach to the study of  
981 bonebeds. In: Rogers, R. R., Eberth, D. A., Fiorillo, A. R. (Eds.), *Bonebeds. Genesis,*  
982 *Analysis, and Paleobiological Significance*. The University of Chicago Press, pp.  
983 265–332.
- 984 Enloe, J. G., 2006. Geological processes and site structure: assessing integrity at a late  
985 paleolithic open-air site in northern france. *Geoarchaeology* 21 (6), 523–540.
- 986 Eren, M. I., Durant, A., Neudorf, C., Haslam, M., Shipton, C., Bora, J., Korisettar,  
987 R., Petraglia, M., 2010. Experimental examination of animal trampling effects on  
988 artifact movement in dry and water saturated substrates: a test case from South India.  
989 *Journal of Archaeological Science* 37 (12), 3010 – 3021.
- 990 Fernández-López, S. R., 1991. Taphonomic concepts for a theoretical biochronology.  
991 *Revista Española de Paleontología* 6, 37–49.
- 992 Fiorillo, A. R., 1991. Taphonomy and depositional setting of careless creek quarry (ju-  
993 dith river formation), wheatland county, montana, u.s.a. *Palaeogeography, Palaeo-  
994 climatology, Palaeoecology* 81 (3), 281–311.
- 995 García-Moreno, A., Smith, G. M., Kindler, L., Pop, E., Roebroeks, W., Gaudzinski-  
996 Windheuser, S., Klinkenberg, V., 2016. Evaluating the incidence of hydrological  
997 processes during site formation through orientation analysis. A case study of the  
998 middle Palaeolithic Lakeland site of Neumark-Nord 2 (Germany). *Journal of Ar-  
999 chaeological Science: Reports* 6, 82 – 93.

- 1000 Giusti, D., Arzarello, M., 2016. The need for a taphonomic perspective in spatial analy-  
1001 sis: Formation processes at the Early Pleistocene site of Pirro Nord (P13), Apricena,  
1002 Italy. *Journal of Archaeological Science: Reports* 8, 235 – 249.
- 1003 Harvati, K., Panagopoulou, E., Tourloukis, V., Thompson, N., Karkanas, P., Athanasi-  
1004 siou, A., Konidaris, G., Tsartsidou, G., Giusti, D., 2016. New Middle Pleistocene  
1005 elephant butchering site from Greece. In: Paleoanthropology Society Meeting. At-  
1006 lanta, Georgia, pp. A14–A15.
- 1007 Hivernel, F., Hodder, I., 1984. Analysis of artifact distribution at Ngenym (Kenya):  
1008 depositional and postdepositional effects. In: Hietala, H., Larson, P. (Eds.), *Intrasite*  
1009 *Spatial Analysis in Archaeology*. Cambridge University Press, Ch. 7, pp. 97–115.
- 1010 Hodder, I., Orton, C., 1976. *Spatial Analysis in Archaeology. New Studies in Archaeo-*  
1011 *logy*. Cambridge University Press, Cambridge.
- 1012 Hovers, E., Ekshtain, R., Greenbaum, N., Malinsky-Buller, A., Nir, N., Yeshurun, R.,  
1013 2014. Islands in a stream? Reconstructing site formation processes in the late Middle  
1014 Paleolithic site of 'Ein Qashish, northern Israel. *Quaternary International* 331, 216–  
1015 233.
- 1016 Isaac, G. L., 1967. Towards the interpretation of occupation debris: Some experiments  
1017 and observations. *Kroeber Anthropological Society Papers* 37 (37), 31–57.
- 1018 Jammalamadaka, S., Sengupta, A., Sengupta, A., 2001. *Topics in Circular Statistics.*  
1019 Series on multivariate analysis. World Scientific.
- 1020 Karkanas, P., Tourloukis, V., Thompson, N., Giusti, D., Panagopoulou, E., Harvati, K.,  
1021 this issue. Sedimentology and micromorphology of the lower palaeolithic lakeshore  
1022 site marathousa 1, megalopolis basin, greece. *Quaternary International*.
- 1023 Kluskens, S. L., 1990. Orientation and density analysis of stone artefacts at combe-  
1024 capelle bas, périgord, france. Master's thesis, University of Pennsylvania.
- 1025 Konidaris, G., Athanassiou, A., Tourloukis, V., Thompson, N., Giusti, D.,  
1026 Panagopoulou, E., Harvati, K., this issue. The elephas (*palaeoloxodon*) antiquus  
1027 skeleton and other large mammals from the lower palaeolithic locality marathousa-  
1028 1 (megalopolis basin, greece): preliminary results on taxonomy, biochronology,  
1029 palaeoecology and taphonomy. *Quaternary International*.
- 1030 Krumbein, W. C., 1941. Measurement and geological significance of shape and  
1031 roundness of sedimentary particles. *JOURNAL OF SEDIMENTARY PETROLOGY*  
1032 11 (2), 64–72.
- 1033 Lenoble, A., Bertran, P., 2004. Fabric of Palaeolithic levels: methods and implications  
1034 for site formation processes. *Journal of Archaeological Science* 31 (4), 457 – 469.
- 1035 Lenoble, A., Bertran, P., Lacrampe, F., 2008. Solifluction-induced modifications  
1036 of archaeological levels: simulation based on experimental data from a modern  
1037 periglacial slope and application to French Palaeolithic sites. *Journal of Archaeo-*  
1038 *logical Science* 35 (1), 99 – 110.

- 1039 Lindsay, J. F., 1968. The development of clast fabric in mudflows. *Journal of Sedimentary Research* 38 (4), 1242–1253.
- 1040
- 1041 Macdonald, D. I. M., Jefferson, T. H., 1985. Orientation studies of waterlogged wood;  
1042 a paleocurrent indicator? *Journal of Sedimentary Research* 55 (2), 235–239.
- 1043 Malinsky-Buller, A., Hovers, E., Marder, O., 2011. Making time: ‘Living floors’,  
1044 ‘palimpsests’ and site formation processes – A perspective from the open-air Lower  
1045 Paleolithic site of Revadim Quarry, Israel. *Journal of Anthropological Archaeology*  
1046 30 (2), 89 – 101.
- 1047 Marwick, B., 2017. Computational reproducibility in archaeological research: Ba-  
1048 sic principles and a case study of their implementation. *Journal of Archaeological  
1049 Method and Theory* 24 (2), 424–450.
- 1050 Marwick, B., d’Alpoim Guedes, J., Barton, C. M., Bates, L. A., Baxter, M., Beavan,  
1051 A., Bollwerk, E. A., Bocinsky, R. K., Brughams, T., Carter, A. K., Conrad, C.,  
1052 Contreras, D. A., Costa, S., Crema, E. R., Daggett, A., Davies, B., Drake, B. L.,  
1053 Dye, T. S., France, P., Fullager, R., Giusti, D., Graham, S., Harris, M. D., Hawks, J.,  
1054 Heath, S., Huffer, D., Kansa, E. C., Kansa, S. W., Madsen, M. E., Melcher, J., Negre,  
1055 J., Neiman, F. D., Opitz, R., Orton, D. C., Przystupa, P., Raviele, M., Riel-Salvatore,  
1056 J., Riris, P., Romanowska, I., Smith, J., Strupler, N., Ullah, I. I., Vlack, H. G. V.,  
1057 VanValkenberg, N., Watrall, E. C., Webster, C., Wells, J., Winters, J., Wren, C. D.,  
1058 2017. Open science in archaeology. *SAA Archaeological Record* 17 (4), 8–14.
- 1059 McPherron, S. J., 2005. Artifact orientations and site formation processes from total  
1060 station proveniences. *Journal of Archaeological Science* 32 (7), 1003 – 1014.
- 1061 McPherron, S. J., Dibble, H. L., Goldberg, P., 2005. Z. *Geoarchaeology* 20 (3), 243–  
1062 262.
- 1063 Morton, A. G. T., 2004. Archaeological Site Formation: Understanding Lake Margin  
1064 Contexts. No. 1211 in BAR International Series. Archaeopress, Oxford.
- 1065 Nickel, B., Riegel, W., Schonherr, T., Velitzelos, E., 1996. Environments of coal forma-  
1066 tion in the Pleistocene lignite at Megalopolis, Peloponnese (Greece) - reconstruc-  
1067 tion from palynological and petrological investigations. *N. Jb. Geol. Palaont. A.* 200,  
1068 201–220.
- 1069 Ohser, J., 1983. On estimators for the reduced second moment measure of point pro-  
1070 cesses. *Mathematische Operationsforschung und Statistik, series Statistics* 14, 63–  
1071 71.
- 1072 Organista, E., Domínguez-Rodrigo, M., Yravedra, J., Uribelarrea, D., Arriaza, M. C.,  
1073 Ortega, M. C., Mabulla, A., Gidna, A., Baquedano, E., 2017. Biotic and abiotic pro-  
1074 cesses affecting the formation of BK Level 4c (Bed II, Olduvai Gorge) and their bear-  
1075 ing on hominin behavior at the site. *Palaeogeography, Palaeoclimatology, Palaeo-  
1076 ecology*, –.

- 1077 Orton, C., 1982. Stochastic process and archaeological mechanism in spatial analysis.  
1078 *Journal of Archaeological Science* 9 (1), 1 – 23.
- 1079 Panagopoulou, E., Tourloukis, V., Thompson, N., Athanassiou, A., Tsartsidou, G.,  
1080 Konidaris, G., Giusti, D., Karkanas, P., Harvati, K., 2015. Marathousa 1: a new Mid-  
1081 dle Pleistocene archaeological site from Greece. *Antiquity Project Gallery* 89 (343).
- 1082 Petraglia, M. D., Nash, D. T., 1987. The impact of fluvial processes on experimen-  
1083 tal sites. In: Nash, D. T., Petraglia, M. D. (Eds.), *Natural formation processes and*  
1084 *the archaeological record*. Vol. 352 of *International Series. British Archaeological*  
1085 *Reports*, Oxford, pp. 108–130.
- 1086 Petraglia, M. D., Potts, R., 1994. Water Flow and the Formation of Early Pleistocene  
1087 Artifact Sites in Olduvai Gorge, Tanzania . *Journal of Anthropological Archaeology*  
1088 13 (3), 228 – 254.
- 1089 Pierson, T. C., 2005. Distinguishing between debris flows and floods from field evi-  
1090 dence in small watersheds. *Usgs numbered series, U.S. Geological Survey*.
- 1091 R Core Team, 2017. R: A Language and Environment for Statistical Computing. R  
1092 Foundation for Statistical Computing, Vienna, Austria.  
1093 URL <https://www.R-project.org/>
- 1094 Ripley, B., 1977. Modelling spatial patterns. *Journal of the Royal Statistical Society,*  
1095 *series B* 39, 172–212.
- 1096 Ripley, B., 1988. Statistical inference for spatial processes. Cambridge University  
1097 Press.
- 1098 Ripley, B. D., 1976. The second-order analysis of stationary point processes. *Journal*  
1099 *of Applied Probability* 13 (2), 255–266.
- 1100 Ripley, B. D., 1981. Spatial Statistics. John Wiley and Sons, New York.
- 1101 Schick, K. D., 1984. Processes of paleolithic site formation: an experimental study.  
1102 Ph.D. thesis, University of California, Berkeley.
- 1103 Schick, K. D., 1986. Stone Age sites in the making: experiments in the formation  
1104 and transformation of archaeological occurrences. Vol. 319 of *International Series.*  
1105 *British Archaeological Reports*, Oxford.
- 1106 Schick, K. D., 1987. Modeling the formation of Early Stone Age artifact concentra-  
1107 tions. *Journal of Human Evolution* 16, 789–807.
- 1108 Schiffer, M. B., 1972. Archaeological Context and Systemic Context. *American Antiq-*  
1109 *uity* 37 (2), 156–165.
- 1110 Schiffer, M. B., 1983. Toward the identification of formation processes. *American An-*  
1111 *tiquity* 48 (4), 675–706.

- 1112 Schiffer, M. B., 1987. Formation processes of the archaeological record. University of  
1113 New Mexico Press, Albuquerque.
- 1114 Shackley, M. L., 1978. The behaviour of artefacts as sedimentary particles in a fluvialite  
1115 environment. *Archaeometry* 20 (1), 55–61.
- 1116 Sánchez-Romero, L., Benito-Calvo, A., Pérez-González, A., Santonja, M., 12 2016.  
1117 Assessment of Accumulation Processes at the Middle Pleistocene Site of Ambrona  
1118 (Soria, Spain). Density and Orientation Patterns in Spatial Datasets Derived from  
1119 Excavations Conducted from the 1960s to the Present. *PLOS ONE* 11 (12), 1–27.
- 1120 Texier, J.-P., 2000. A propos des processus de formation des sites préhistoriques / About  
1121 prehistoric site formation processes. *Paléo* 12 (1), 379–386.
- 1122 Toots, H., 1965. Orientation and distribution of fossils as environmental indicators. In: Nineteenth Field Conference of the Wyoming Geological Association. pp. 219–292.
- 1124 Tourloukis, V., Thompson, N., Panagopoulou, E., Giusti, D., Konidaris, G., Karkanas,  
1125 P., Harvati, K., this issue. Lithic and osseous artifacts from the lower palaeolithic site  
1126 of marathousa 1, megalopolis, greece: preliminary results. *Quaternary International*.
- 1127 van Vugt, N., de Brujin, H., van Kolfschoten, M., Langereis, C. G., 2000. Magneto-  
1128 and cyclostratigraphy and mammal-fauna's of the Pleistocene lacustrine Megalopo-  
1129 lis Basin, Peloponnesos, Greece. *Geologica Ultrajectina* 189, 69–92.
- 1130 Vaquero, M., Chacón, M. G., García-Antón, M. D., de Soler, B. G., Martínez, K.,  
1131 Cuartero, F., 2012. Time and space in the formation of lithic assemblages: The  
1132 example of Abric Romaní Level J. *Quaternary International* 247 (0), 162 – 181.
- 1133 Villa, P., 2004. Taphonomy and stratigraphy in european prehistory. *Before Farming*  
1134 2004 (1), 1–20.
- 1135 Voorhies, M., 1969. Taphonomy and population dynamics of an early pliocene vertebrate  
1136 fauna, knox county, nebraska. *Contributions to Geology, University of*  
1137 *Wyoming Special Paper* 1, 1–69.
- 1138 Walter, M. J., Trauth, M. H., 2013. A {MATLAB} based orientation analysis of  
1139 acheulean handaxe accumulations in olorgesailie and kariandusi, kenya rift. *Journal*  
1140 *of Human Evolution* 64 (6), 569 – 581.
- 1141 Wood, R. W., Johnson, D. L., 1978. A survey of disturbance processes in archaeological  
1142 site formation. In: Schiffer, M. B. (Ed.), *Advances in archaeological method and*  
1143 *theory*. Vol. 1. Academic Press, Ch. 9, pp. 315–381.
- 1144 Woodcock, N., Naylor, M., 1983. Randomness testing in three-dimensional orientation  
1145 data. *Journal of Structural Geology* 5 (5), 539 – 548.